OPEN ACCESS
IOP Publishing
Journal of Physics A: Mathematical and Theoretical
J. Phys. A: Math. Theor. **58** (2025) 115302 (30pp)
https://doi.org/10.1088/1751-8121/adb402

Semi-classical limit of the Dirac equation in curved space and applications to strained and photonic graphene

François Fillion-Gourdeau[1,2], **Emmanuel Lorin**[3,4,*], **Steve MacLean**[1,2] **and Xu Yang**[5]

[1] Infinite Potential Laboratories, Waterloo, Ontario N2L 0A9, Canada
[2] Advanced Laser Light Source (ALLS), INRS-Énergie, Matériaux et Télécommunications, Varennes, Québec J3X 1S2, Canada
[3] School of Mathematics and Statistics, Carleton University, Ottawa, Canada
[4] Centre de Recherches Mathématiques, Université de Montréal, Montréal, Canada
[5] Department of Mathematics, University of California, Santa Barbara, CA 93106, United States of America

E-mail: elorin@math.carleton.ca, francois.fillion@inrs.ca, steve.maclean@inrs.ca and xuyang@math.ucsb.edu

Received 10 July 2024; revised 23 January 2025
Accepted for publication 7 February 2025
Published 17 March 2025

Abstract

The semi-classical regime of static Dirac matter is derived from the Dirac equation in curved space-time. The leading- and next-to-leading-order contributions to the semi-classical approximation are evaluated. While the leading-order yields classical equations of motion with relativistic Lorentz and a geometric forces related to space curvature, the next-to-leading-order gives a transport-like equation with source terms. We apply the proposed strategy to the simulation of electron propagation on strained graphene surfaces, as well as to the dynamics of edge states in photonic graphene.

Keywords: semi-classical analysis, graphene, Dirac equation in curved space

* Author to whom any correspondence should be addressed.

1. Introduction

The Dirac equation is at the core of our understanding of matter, being the generalization of the Schrödinger equation for relativistic spin-1/2 particles. Originally, this equation was applied to the theoretical description of elementary particles like electrons or quarks, for high energy physics applications where relativistic effects are important. However, with the advent of some new materials and their effective low-energy description, the Dirac equation has an even more widespread field of application which also includes condensed matter physics. Dirac matter [1, 2] encompasses all quantum systems theoretically described by the Dirac equation such as relativistic fermions, but now includes many quantum materials such as graphene [3–5], and more generally topological insulators [6–8], Dirac semimetals [9], some high-temperature supraconductors [10] and liquid Helium-3 [11]. It also includes exotic structures such as artificial graphene [12], photonic graphene analogs [13–16], photonic topological insulators [17] and phononic metamaterials [18]. Many of these materials are in the class of two-dimensional materials, where the underlying symmetry of the cristal lattice makes for a relativistic-like description of quasi-particles in the low-energy limit.

Understanding the properties of such systems is a theoretical problem requiring explicit solutions to the Dirac equation. Numerical and analytical methods have been developed to achieve such a feat [19–28], but it still remains a challenging task. Assuming the external potentials are smooth enough, an interesting alternative is to use the semi-classical approximation, in which the problem reduces to the solution of a classical-like system of equations [29]. This approach has been implemented on the Dirac equation to understand and describe the relativistic quantum dynamics of fermions under various external fields [29–34]. Motivated by applications such as the Dirac fermion microscope [35], the semi-classical technique has also been applied to charge carriers in graphene [36–38] for analyzing Veselago lenses [39]. This gave rise to the field of 'electron optics' in graphene, where ray-optics can be used to understand the behavior of electrons in Dirac materials.

In comparison, less work has been performed on the semi-classical limit of the curved space Dirac equation [40–44], possibly because the coupling to a gravitational field increases technical complications. Nevertheless, the curved space Dirac equation is also relevant for the description of systems in condensed matter, such as strained graphene [45–51] or more generally, for straintonics in Dirac materials. In this approach, electron control can be achieved by mechanical deformations, permitting the focusing [27, 52] or confinement [28] of charge carriers.

In this article, the semi-classical limit of static Dirac matter is investigated in the general case where the quantum system is described by the curved space Dirac equation with a space-dependent mass gap. Thus, it provides a general framework to investigate the behavior of fermions in numerous physical systems.

Interestingly, the general form of the Dirac operator studied in this paper is also relevant for the propagation of edge states in photonic graphene [53]. Edge states are particular solutions to the Maxwell equations in photonic graphene (an optical analogue to graphene) which propagate along 'walls/interface' at some surface boundary. In this setting, the Maxwell equations can actually be rewritten in the form of a Schrödinger equation with periodic coefficients, from which it is possible to derive a Dirac equation with space-dependent mass (wall-function) describing edge states dynamics. The semi-classical limit of the Dirac equation yields a simple theoretical framework to describe this physical system while keeping the main important properties of edge state dynamics.

1.1. Theoretical model of Dirac matter: curved-space Dirac equation

Dirac matter shall be defined here as any quantum systems whose fermionic degrees of freedom are characterized by the Dirac equation in curved-space. We are assuming the mostly-plus flat space metric: $\eta_{AB} = \mathrm{diag}[-1,1,1,1]$.

In covariant form, the curved-space Dirac equation is given by [47, 54, 55]

$$[\hbar\bar{\gamma}^{\mu}(x)D_{\mu} + m_D(x)v_D]\psi(x) = 0, \tag{1}$$

where $\psi(x)$ is the two-component (in 1-D and 2D) or four-component (in 3D) spinor wavefunction, m_D is the (space-dependent) mass of the fermion state, v_D is the Dirac velocity, $x = (t,\boldsymbol{x})$ is a set of curvilinear coordinates (bold symbols are spatial vectors) and $\bar{\gamma}(x) = (\bar{\gamma}^0(x), \bar{\gamma}^i(x))$ are the generalized gamma matrices. A curved-space manifold is associated to such systems via the generalized gamma matrices isomorphic to the local Clifford algebra such that

$$\{\bar{\gamma}^{\mu}(x), \bar{\gamma}^{\nu}(x)\} = 2g^{\mu\nu}(x), \tag{2}$$

which can be written in terms of the vielbein as $\bar{\gamma}^{\mu}(x) = e^{\mu}_{A}(x)\gamma^{A}$, where γ^{A} are the standard flat-space Dirac matrices (uppercase indices are flat space Lorentz indices). As usual, $g^{\mu\nu}(x)$ is the metric of the space-time manifold. Finally, the expression

$$D_{\mu} = \partial_{\mu} + \Omega_{\mu} - \mathtt{i}\frac{q}{v_D\hbar}A_{\mu}(x)$$

stands for the curved-space covariant derivative where A_{μ} represents the coupling to a vector field and

$$\Omega_{\mu}(x) = \frac{1}{4}\omega^{AB}_{\mu}(x)\gamma_A\gamma_B, \tag{3}$$

where the spin connection is

$$\omega^{AB}_{\mu}(x) = e^{A}_{\nu}(x)g^{\nu\lambda}(x)\left[\partial_{\mu}e^{B}_{\lambda}(x) - \Gamma^{\sigma}_{\mu\lambda}(x)e^{B}_{\sigma}(x)\right]. \tag{4}$$

Here, the Christoffel symbols are given as usual by

$$\Gamma^{\nu}_{\mu\sigma}(x) = \frac{g^{\nu\rho}(x)}{2}\left[\partial_{\sigma}g_{\rho\mu}(x) + \partial_{\mu}g_{\rho\sigma}(x) - \partial_{\rho}g_{\mu\sigma}(x)\right]. \tag{5}$$

Specializing this formulation to static manifolds, the most general metric yields a line element of the form

$$ds^2 = -\left(dx^0\right)^2 + d\boldsymbol{x}\cdot d\boldsymbol{x}, \tag{6}$$

$$= -v_D^2dt^2 + g_{ij}(\boldsymbol{x})dx^idx^j, \tag{7}$$

where g^{ij} are the components of the 'spatial' metric tensor. It is possible to write the Dirac equation (1) in a Schrödinger-like form in Cartesian coordinates for a general geometry characterized by the metric (6). The Dirac equation reads:

$$\left[\mathtt{i}\hbar\bar{\gamma}^0D_0 + \mathtt{i}\hbar\bar{\gamma}^iD_i + \mathtt{i}m_Dv_D\right]\psi = 0. \tag{8}$$

Using $\bar{\gamma}^0 = \gamma^0$ in the static case, and the fact that $\gamma^0\gamma^0 = -\mathbb{I}_2$ and $\gamma^0 = -\mathtt{i}\beta$, we get

$$\left[-\mathtt{i}\hbar\left(\partial_0 - \mathtt{i}\frac{q}{\hbar v_D}A_0\right) + \mathtt{i}\hbar\gamma^0\bar{\gamma}^i D_i + \mathtt{i}m_D v_D\gamma^0\right]\psi = 0. \tag{9}$$

As

$$\frac{d}{dx^0} = \frac{dt}{dx^0}\frac{d}{dt} = \frac{1}{v_D}\frac{d}{dt},$$

and $A_0 = g_{00}A^0 = -V$, we get

$$\left[-\mathtt{i}\frac{\hbar}{v_D}\left(\partial_t + \mathtt{i}\frac{q}{\hbar}V\right) + \mathtt{i}\hbar\gamma^0\bar{\gamma}^i D_i + \mathtt{i}m_D v_D\gamma^0\right]\psi = 0. \tag{10}$$

Finally, using $\gamma^0 = -\mathtt{i}\beta$ and $\gamma^0\bar{\gamma}^i = -\bar{\alpha}_i$, the Dirac equation becomes

$$\mathtt{i}\hbar\partial_t\psi(t,\boldsymbol{x}) = \left[-\mathtt{i}\hbar v_D\bar{\alpha}^i(\boldsymbol{x})D_i + m_D(\boldsymbol{x})v_D^2\beta + qV(\boldsymbol{x})\right]\psi(t,\boldsymbol{x}), \tag{11}$$

where $V = -A_0$ is the scalar potential and $\bar{\alpha}^i(\boldsymbol{x}) = e^i_a(\boldsymbol{x})\gamma^0\gamma^a$ are the generalized Dirac matrices. A standard representation of Dirac matrices is chosen, with $\alpha^a = \sigma^a$ (for $a = 1,2$) and $\beta = \sigma^3$ (σ^i are Pauli matrices) in 1D or 2D, and $\alpha^a = \sigma_x \otimes \sigma^a$ (for $a = 1,2,3$) and $\beta = \sigma^3 \otimes \mathbb{I}_2$ in 3D. The gauge field A_i can be an external electromagnetic field or can emerge from the low energy limit of a more complete model (for example, in strained graphene, this is obtained from the low-energy limit of the tight-binding model and the gauge field is interpreted as a pseudo-magnetic field [50]).

1.2. Organization of the paper

The semi-classical limit of the Dirac equation in curved-space that models Dirac matter is derived in section 2. The methodology developed in this paper is applied to the propagation of wavepackets on strained graphene surfaces in section 3, and then to the evolution of edge states in photonic graphene in section 4. Some mathematical properties and numerical experiments will also be proposed. Finally, we conclude in section 5.

2. Semi-classical limit

To simplify the notation, we now introduce the relevant functional spaces, assuming that d is the number of spatial dimensions. We recall that the Sobolev space $H^1(\Omega;\mathbb{C}^{s_d})$ represents the Hilbert space of $L^2(\Omega;\mathbb{C}^{s_d})$-functions, with derivatives which also belong to $L^2(\Omega;\mathbb{C}^{s_d})$. The Hilbert space of H^1-functions which are null at the boundary of Ω, is denoted by $H^1_0(\Omega;\mathbb{C}^{s_d})$. We set $X = H^1_0(\Omega;\mathbb{C}^{s_d})$, $Y_0 = C^1(\Omega;\mathbb{R})$, $Y_1 = C^1(\Omega;\mathbb{R}^{s_d})$, $Y_2 = C^1(\Omega;\mathbb{C}^{s_d\times s_d})$, where $\Omega \subset \mathbb{R}^d$ is the (semi-)bounded domain and where $s_d = 2$ for $d = 1,2$, or $s_d = 4$ for $d = 3$. If $\Omega = \mathbb{R}^d$, we set $X = H^1(\mathbb{R}^2;\mathbb{C}^{s_d})$, $Y_0 = C^1_b(\mathbb{R}^d;\mathbb{R})$, $Y_1 = C^1_b(\mathbb{R}^d;\mathbb{R}^{s_d})$, $Y_2 = C^1_b(\mathbb{R}^d;\mathbb{C}^{s_d\times s_d})$, where C^1_b is the set of continuously differential functions with compact support (that is with non-zero values only within a bounded region). We denote $(\cdot,\cdot)_X$ the inner product on X, such that for any u and v in X

$$(u,v)_X = \int_\Omega u(\boldsymbol{x})v^*(\boldsymbol{x})\,d\boldsymbol{x} + \sum_{i=1}^d\int_\Omega \partial_i u(\boldsymbol{x})\,\partial_i v^*(\boldsymbol{x})\,d\boldsymbol{x}.$$

Potential V will be assumed to belong to Y or $Z_0 = H^1(\Omega;\mathbb{R}^{s_d})$.

The starting point of the derivation is the Dirac equation in Schrödinger-like form given by equation (11). Then, this equation is adimensionalized by introducing scaled coordinates $t' = t/t_s$ and $\boldsymbol{x}' = \boldsymbol{x}/x_s$, where t_s, x_s are arbitrary time and space scales. The potentials are also scaled as $A_i(\boldsymbol{x}) = A_s\tilde{A}_i(\boldsymbol{x}')$ and $V(\boldsymbol{x}) = A_s\tilde{V}(\boldsymbol{x}')$, where A_s is the unit potential scale. Then, the Dirac equation becomes

$$\begin{aligned}\mathtt{i}\varepsilon\partial_t\psi(t,\boldsymbol{x}) = \big\{&-\mathtt{i}\varepsilon\bar{\alpha}^i(\boldsymbol{x})\left[\partial_i + \Omega_i(\boldsymbol{x})\right] - \bar{\alpha}^i(\boldsymbol{x})\tilde{A}_i(\boldsymbol{x}) \\ &+\tilde{m}_D(\boldsymbol{x})\beta + \tilde{V}(\boldsymbol{x})\mathbb{I}_2\big\}\psi(t,\boldsymbol{x}),\end{aligned} \tag{12}$$

where we set the time scale to $t_s = x_s/v_D$ and the adimensional mass to $\tilde{m}_D(\boldsymbol{x}) = v_D^2 m_D(\boldsymbol{x})/qA_s$. The semi-classical parameter is then defined as

$$\varepsilon = \frac{\hbar v_D}{x_s q A_s}. \tag{13}$$

The semi-classical limit hence corresponds to $\varepsilon \to 0$. In the following, an asymptotic expansion in this regime will be derived. For this purpose, we insert the ansatz

$$\psi(t,\boldsymbol{x}) = \exp\left(\mathtt{i}\frac{S(t,\boldsymbol{x})}{\varepsilon}\right)\sum_{n=0}^{\infty}\left(\frac{\varepsilon}{\mathtt{i}}\right)^n u_n(t,\boldsymbol{x}), \tag{14}$$

into equation (12), where the amplitudes u_n are spinors and $S \in \mathbb{R}$ is the phase [29]. Then, we define the following operators:

$$\mathcal{G}(t,\boldsymbol{x}) = \partial_t S(t,\boldsymbol{x}) + \bar{\alpha}^i(\boldsymbol{x})\pi_i + \beta\tilde{m}_D(\boldsymbol{x}) + \tilde{V}(\boldsymbol{x}), \tag{15}$$

$$\mathcal{H}(\boldsymbol{x}) = \partial_t + \bar{\alpha}^i(\boldsymbol{x})\left[\partial_i + \Omega_i(\boldsymbol{x})\right]. \tag{16}$$

Order by order, the semi-classical expansion is then written as (for $n \geqslant 1$)

$$\mathcal{G}u_0 = 0, \tag{17}$$

$$\mathcal{G}u_n = -\mathcal{H}u_{n-1}, \tag{18}$$

where the kinematic momentum is defined as $\pi_i := \partial_i S - \tilde{A}_i$.

In the following, we will denote $\bar{\boldsymbol{\alpha}} = [\bar{\alpha}^k]_{k=1,\cdots,d}^T$ and $\boldsymbol{X}\cdot\boldsymbol{Y} = \sum_{i,j=1}^d g_{ij}X^iY^j$ for arbitrary $\boldsymbol{X}$ and $\boldsymbol{Y}$. We denote $\nabla_{\boldsymbol{x}}\bar{\boldsymbol{\alpha}} = \{\partial_i\bar{\alpha}^j\}_{ij}$, and $\boldsymbol{\Gamma} = \{\Gamma_k\}_k$ where the Christophel symbols $\Gamma_k = \{\Gamma^j_{ki}\}_{ij}$ are defined in (5).

The semi-classical limit is summarized in the following theorem.

Theorem 2.1. *Consider a smooth domain Ω (with C^1-boundary if Ω bounded), and we denote by g the corresponding smooth metric tensor. For $\varepsilon > 0$, we consider the adimensionalized Dirac equation on $\Omega \times [0,T]$*

$$\mathtt{i}\varepsilon\partial_t\psi(t,\boldsymbol{x}) = \left\{-\mathtt{i}\varepsilon\bar{\boldsymbol{\alpha}}(\boldsymbol{x})\cdot\left[\nabla + \boldsymbol{\Omega}(\boldsymbol{x})\right] - \bar{\boldsymbol{\alpha}}(\boldsymbol{x})\cdot\tilde{\boldsymbol{A}}(\boldsymbol{x}) + \tilde{m}_D(\boldsymbol{x})\beta + \tilde{V}(\boldsymbol{x})\mathbb{I}_2\right\}\psi(t,\boldsymbol{x}), \tag{19}$$

with i) $\psi_0 \in X$, ii) $\tilde{m}_D \in C^1((0,T];Y_0)$, $\tilde{\boldsymbol{A}} \in C^1((0,T];Y_1)$, $\bar{\boldsymbol{\alpha}} \in C^1((0,T];Y_2 \otimes Y_2)$ and $\tilde{V} \in Z$. Considering the solution in the form

$$\psi(t,\boldsymbol{x}) = \exp\left(\mathtt{i}\frac{S(t,\boldsymbol{x})}{\varepsilon}\right)\sum_{n=0}^{\infty}\left(\frac{\varepsilon}{\mathtt{i}}\right)^n u_n(t,\boldsymbol{x}),$$

with $\varepsilon \to 0$, we deduce from the leading-order (LO) and next-to-leading-order (NLO) asymptotic expansion, the following equations:

- *Equation of motion.*

$$\frac{d\boldsymbol{x}}{dt} = \pm\frac{\boldsymbol{\pi}(t,\boldsymbol{x})}{\lambda(t,\boldsymbol{x})},$$
$$\frac{d\boldsymbol{\pi}}{dt} = \boldsymbol{F}_{\text{mass}} + \boldsymbol{F}_{\text{geom}} + \boldsymbol{F}_{\text{mass}},$$

  where $\boldsymbol{\pi} = \nabla_{\boldsymbol{x}} S - \boldsymbol{A}$, $\lambda(t,\boldsymbol{x}) = \sqrt{(g^{-1}(\boldsymbol{x})\boldsymbol{\pi})\boldsymbol{\pi} + \tilde{m}_D^2(\boldsymbol{x})}$ and

$$\boldsymbol{F}_{\text{geom}} = \boldsymbol{\pi}\mathbb{I}_2(\boldsymbol{\Gamma}\dot{\boldsymbol{x}}),$$
$$\boldsymbol{F}_{\text{lorentz}} = \boldsymbol{E}(\boldsymbol{x}) + \dot{\boldsymbol{x}} \times \boldsymbol{B}(\boldsymbol{x}),$$
$$\boldsymbol{F}_{\text{mass}} = \mp\frac{\nabla_{\boldsymbol{x}}\tilde{m}_D^2(\boldsymbol{x})}{\lambda(t,\boldsymbol{x})},$$

  where $\boldsymbol{E} = -\nabla_{\boldsymbol{x}} V - \partial_t \boldsymbol{A}, \boldsymbol{B} = \nabla_{\boldsymbol{x}} \times \boldsymbol{A}$ are respectively the electric and magnetic fields associated to $\boldsymbol{A}$.
- *Eikonal equation.*

$$\partial_t S^{\pm}(t,\boldsymbol{x}) \pm \lambda(t,\boldsymbol{x}) + \tilde{V}(\boldsymbol{x}) = 0.$$

- *Transport equations. The set of uncoupled transport equations is given by*

$$\Big[\partial_t + \boldsymbol{\omega}_{\pm}\nabla_{\boldsymbol{x}} + \bar{\boldsymbol{\alpha}}\cdot\boldsymbol{\Omega} - \frac{1}{\lambda}\boldsymbol{\omega}_{\pm}\nabla_{\boldsymbol{x}}\lambda \pm \frac{1}{2\lambda}\left((\bar{\boldsymbol{\alpha}}\cdot\nabla_{\boldsymbol{x}}\tilde{m}_D)\beta + \boldsymbol{\omega}_{\pm}\nabla_{\boldsymbol{x}}\tilde{m}_D\beta\right) +$$
$$\pm\frac{1}{2\lambda}(\bar{\boldsymbol{\alpha}}\cdot\nabla_{\boldsymbol{x}})(\bar{\boldsymbol{\alpha}}\cdot\boldsymbol{\pi}) \pm \frac{1}{2\lambda}\boldsymbol{\omega}_{\pm}\nabla_{\boldsymbol{x}}\boldsymbol{\pi}^T\boldsymbol{\omega}_{\pm} \pm \frac{1}{2\lambda}\left(\nabla_{\boldsymbol{x}}\bar{\boldsymbol{\alpha}}^T M\boldsymbol{\pi}\right)\cdot\bar{\boldsymbol{\omega}}_{\pm}\Big] u_{0,\pm} = 0,$$

  where $\boldsymbol{\omega}_{\pm} = \pm\boldsymbol{\pi}/\lambda$ and $M = (\mathbb{I}_2, \mathbb{I}_2) \in \mathbb{R}^{4\times 2}$.

Proof. The derivation of the eikonal and motion equations is obtained from the zeroth order expansion in ε, while the transport equation is derived from the first order expansion.

LO in ε. At LO in ε, a dynamical equation for S can be obtained by noticing that equation (17) is a homogeneous system of linear equations ($\mathcal{G}$ is a matrix in spinor space) having a non-trivial solution only if the determinant in spinor space is zero [56]. As $(\partial_t S + \tilde{m}_D + \tilde{V})\mathbb{I}_2$ and $\sigma^a\bar{\pi}_a$ commute, $\det\mathcal{G}$ is given by

$$\begin{aligned}\det\mathcal{G} &= \det\begin{bmatrix}\left(\partial_t S + \tilde{m}_D + \tilde{V}\right)\mathbb{I}_2 & \sigma^a\bar{\pi}_a \\ \sigma^a\bar{\pi}_a & \left(\partial_t S - \tilde{m}_D + \tilde{V}\right)\mathbb{I}_2\end{bmatrix} \\ &= \det\left[\left(\partial_t S + \tilde{m}_D + \tilde{V}\right)\left(\partial_t S - \tilde{m}_D + \tilde{V}\right)\mathbb{I}_2 - \sigma^a\sigma^b\bar{\pi}_a\bar{\pi}_b\right].\end{aligned}$$

Using the fact that $\sigma^a\sigma^b = \delta^{ab} + \mathtt{i}\varepsilon_c^{ab}\sigma^c$, we get

$$\sigma^a\sigma^b\bar{\pi}_a\bar{\pi}_b = \left(\delta^{ab} + \mathtt{i}\varepsilon_c^{ab}\sigma^c\right)\bar{\pi}_a\bar{\pi}_b \tag{20}$$
$$= \eta^{ab}\bar{\pi}_a\bar{\pi}_b = g^{ij}\pi_i\pi_j. \tag{21}$$

Thus we get $\det\mathcal{G} = \det[((\partial_t S + \tilde{V})^2)\mathbb{I}_2 - m_D^2 - g^{ij}\pi_i\pi_j]$, then

$$\det\mathcal{G} = \det\left[\left(\left(\partial_t S + \tilde{V}\right)^2\right)\mathbb{I}_2 - m_D^2 - g^{ij}\pi_i\pi_j\right]^2. \tag{22}$$

This yields two 2-fold degenerate solutions denoted by the index $\pm$:

$$\partial_t S_\pm + h_\pm = 0\,, \tag{23}$$

where we defined the classical Hamiltonian

$$\begin{aligned} h_\pm &= \pm\lambda + \tilde{V}, \\ \lambda &= -\sqrt{g^{ij}\pi_i\pi_j + \tilde{m}_D^2}\,. \end{aligned}$$

The superscript $\pm$ is the band index that stands for positive or negative energy bands. The classical Hamiltonian is the one for a classical relativistic particle in curved space immersed in an electromagnetic field.

Particle-like trajectories can be obtained from the eikonal equation via the method of characteristics. These equations are important physically as trajectories are orthogonal to wavefronts of the wavefunction [57] and thus, are directly related to wave propagation. Letting $p_k = \partial_k S$, the equations of motion are written as

$$\frac{dx^k}{dt} = \frac{\partial h_\pm}{\partial p_k}\,,\ \frac{dp_k}{dt} = -\frac{\partial h_\pm}{\partial x^k}. \tag{24}$$

Explicitly, we have

$$\begin{aligned} \frac{\partial h_\pm}{\partial p_k} &= \pm\frac{\partial}{\partial p_k}\sqrt{g^{ij}\left(p_i - \tilde{A}_i\right)\left(p_j - \tilde{A}_j\right) + \tilde{m}_D^2} && (25)\\ &= \pm\frac{1}{2\lambda}\frac{\partial}{\partial p_k}\left[g^{ij}p_ip_j - g^{ij}p_j\tilde{A}_i - g^{ij}p_i\tilde{A}_j\right] && (26)\\ &= \pm\frac{1}{2\lambda}\left[g^{ij}\delta_i^k p_j + g^{ij}p_i\delta_j^k - g^{ij}\delta_j^k\tilde{A}_i - g^{ij}\delta_i^k\tilde{A}_j\right] && (27)\\ &= \pm\frac{1}{2\lambda}\left[g^{kj}p_j + g^{ik}p_i - g^{ik}\tilde{A}_i - g^{kj}\tilde{A}_j\right] && (28)\\ &= \pm\frac{\pi^k}{\lambda}, && (29) \end{aligned}$$

where $2\pi^k = g^{kj}\pi_j + g^{ik}\pi_i$. Then we have

$$\begin{aligned} \frac{\partial h_\pm}{\partial x^k} &= \pm\frac{\partial}{\partial x^k}\sqrt{g^{ij}\pi_i\pi_j + \tilde{m}_D^2} && (30)\\ &= \pm\frac{1}{2\lambda}\frac{\partial}{\partial x^k}\left[g^{ij}\pi_i\pi_j + \tilde{m}_D^2\right] && (31)\\ &= \pm\frac{1}{2\lambda}\left[\left(\partial_k g^{ij}\right)\pi_i\pi_j + g^{ij}\left(\partial_k\pi_i\right)\pi_j + g^{ij}\pi_i\left(\partial_k\pi_j\right) + 2\tilde{m}_D\left(\partial_k\tilde{m}_D\right)\right] && (32)\\ &= \pm\frac{1}{2\lambda}\left[-\left(\Gamma^i_{kl}g^{lj} + \Gamma^j_{kl}g^{il}\right)\pi_i\pi_j - g^{ij}\left(\partial_k\tilde{A}_i\right)\pi_j\right. \\ &\quad \left. -g^{ij}\pi_i\left(\partial_k\tilde{A}_j\right) + 2\tilde{m}_D\left(\partial_k\tilde{m}_D\right)\right] && (33) \end{aligned}$$

$$= \pm\frac{1}{\lambda}\left[-\Gamma^i_{kl}\pi_i\pi^l - \left(\partial_k\tilde{A}_i\right)\pi^i + \tilde{m}_D\left(\partial_k\tilde{m}_D\right)\right] \tag{34}$$

$$= -\Gamma^i_{kl}\pi_i\frac{dx^l}{dt} - \left(\partial_k\tilde{A}_i\right)\frac{dx^i}{dt} \pm \frac{1}{\lambda}\tilde{m}_D\left(\partial_k\tilde{m}_D\right), \tag{35}$$

where we used the property of the metric $\partial_k g^{ij} = -\Gamma^i_{kl}g^{lj} - \Gamma^j_{kl}g^{il}$. The equations of motion are given by

$$\frac{dx^k}{dt} = \pm\frac{\pi^k}{\lambda}, \tag{36}$$

$$\frac{dp_k}{dt} = \Gamma^i_{kl}\pi_i\frac{dx^l}{dt} + \left(\partial_k\tilde{A}_i\right)\frac{dx^i}{dt} \mp \frac{1}{\lambda}\tilde{m}_D\left(\partial_k\tilde{m}_D\right). \tag{37}$$

As d/dt is a total derivative, we get

$$\frac{d\pi_k}{dt} = \frac{dp_k}{dt} - \frac{d\tilde{A}_k}{dt} \tag{38}$$

$$= \frac{dp_k}{dt} - \frac{d\tilde{A}_k}{dx^i}\frac{dx^i}{dt} \tag{39}$$

$$= \Gamma^i_{kl}\pi_i\frac{dx^l}{dt} + \left(\partial_k\tilde{A}_i - \partial_i\tilde{A}_k\right)\frac{dx^i}{dt} \mp \frac{1}{\lambda}\tilde{m}_D\left(\partial_k\tilde{m}_D\right) \tag{40}$$

$$= \Gamma^i_{kl}\pi_i\frac{dx^l}{dt} + F_{ki}\frac{dx^i}{dt} \mp \frac{1}{\lambda}\tilde{m}_D\left(\partial_k\tilde{m}_D\right). \tag{41}$$

Thus, we get the Lorentz equation in curved space:

$$\frac{d\pi_k}{dt} = F^{\text{geom}}_k + F^{\text{lorentz}}_k + F^{\text{mass}}_k. \tag{42}$$

Equation (42) corresponds to the relativistic Lorentz force equation for a particle immersed in an electromagnetic field with added forces: the geometric gravitational-like force due to geometry of the curved-space and an inertial force related to the space variation of the particle mass:

$$F^{\text{geom}}_k = \Gamma^i_{kj}\pi_i\dot{x}^j, \tag{43}$$

$$F^{\text{lorentz}}_k = F_{k\nu}\dot{x}^\nu, \tag{44}$$

$$F^{\text{mass}}_k = \mp\frac{\tilde{m}_D\partial_k\tilde{m}_D}{\lambda}, \tag{45}$$

where $F_{\mu\nu} = \partial_\mu\tilde{A}_\nu - \partial_\nu\tilde{A}_\mu$ is the electromagnetic tensor. Equation (42) implies that the LO semi-classical approximation yields a theoretical description in terms of classical relativistic trajectories characterized by the Lorentz force equation in curved spacetime (42) with additional force terms and a space-dependent particle velocity. These features of the classical-like trajectories are obviously not present for relativistic particles in flat space and thus, are direct consequences of the space curvature. When the space is flat, the general metric becomes Minkowskian and one recovers equations of motion given in [36, 37].

NLO in ε. At NLO in ε, a dynamical equation can be obtained for the spinor u_0.
Denoting $\mathcal{G} = \mathcal{G}(x)$, we consider

$$\mathcal{G}u_{1\pm} = -\mathcal{H}u_{0\pm},$$

where $\mathcal{G}$ and $\mathcal{H}$ are defined in (15) and (16), respectively. Let us notice that the eigenvalues of the matrix $\mathcal{G}(x)$ for $x=(t,\boldsymbol{x})\in[0,T]\times\Omega$ are given by

$$\mu_{\pm}(x)=\partial_t S(x)+\tilde{V}(\boldsymbol{x})\mp\sqrt{\tilde{m}_D^2(\boldsymbol{x})+g^{ij}(\boldsymbol{x})\pi_i(x)\pi_j(x)}\,.$$

For any fixed $t\in[0,T]$, we assume that $u_0(t,\cdot)$ and $\mathcal{H}u_0(t,\cdot)\in X$ and $\boldsymbol{x}\mapsto\mathcal{G}(t,\boldsymbol{x})$ belongs to Y. In order to derive the transport equation, within the semi-classical limit, the starting point is the following lemma. By abuse of notation we denote hereafter $\mathcal{G}=\mathcal{G}(t,\cdot)$.

Lemma 2.1. *For any fixed $t\in[0,T]$, $\mathcal{G}:X\to X$ is a Fredholm operator, and*

$$(\mathcal{H}u_{0\pm},u_{0\pm})_X=0\,.$$

Proof. Let us sketch the proof which is relatively standard. In the following, we assume that $t\in[0,T]$ is fixed.

- *$\Pi_{\pm}u\in Ker(\mathcal{G})$ for $u\in Ker(\mathcal{G})$.* This is a consequence of the commutation of $\Pi_{\pm}$ and $\mathcal{G}$.
- *Operator $\mathcal{G}$ is continuous.* As $\mathcal{G}(t,\cdot)\in Y$, we deduce from Cauchy-Schwarz the existence of $c=c(t)>0$ such that

$$\|\mathcal{G}u\|_X\leqslant c\|u\|_X\,.$$

- *$\mathcal{G}$ is a compact operator.* For any $B\subset X$ bounded set of X, $\mathcal{G}(B)$ is relatively compact that is $\overline{\mathcal{G}(B)}$ is compact. Equicontinuity and pointwise boundness of the family of operators $\{\mathcal{G}u\,:\,u\in B\}$ come from the global Lipschitz continuity of $\mathcal{G}(t,\cdot)\in Y$.
- *$Ker(\mathcal{G})$ is finite dimensional.* We consider a sequence $\{u_n\}_n\in\mathrm{Ker}(\mathcal{G})\cap B_X$ such that $\|u_n\|_X\leqslant 1$. As X is reflexive, the ball is weakly relatively compact, and there exists a subsequence $\{u_{\phi(n)}\}_n$ weakly convergent to $u\in X$. As $\mathcal{G}$ is compact $\mathcal{G}u_{\phi(n)}$ is strongly convergent to $\mathcal{G}u$. As $\mathcal{G}u_{\phi(n)}=0$, $u\in\mathrm{Ker}(\mathcal{G})$.
- *$Im(\mathcal{G}^{\perp})$ is finite dimensional.* For any $u\in\mathrm{Im}(\mathcal{G}^{\perp})$, $(u,\mathcal{G}v)_X=0$, for any $v\in X$. As $\mathcal{G}$ is self-adjoint $(\mathcal{G}u,v)=0$ for any $v\in X$, so that $\mathcal{G}u=0$. Hence $\mathrm{Im}(\mathcal{G}^{\perp})\subset\mathrm{Ker}(\mathcal{G})$ is finite dimensional.

This concludes the proof. □

Let us notice that for $u_0\in X$, and decomposing $u_0=\Pi_+u_0+\Pi_-u_0$,

$$(\mathcal{H}u_0,u_0)_X=(\mathcal{H}\Pi_{\pm}u_0,\Pi_{\pm}u_0)_X+(\mathcal{H}\Pi_{\pm}u_0,\Pi_{\mp}u_0)_X\,.$$

The next step consists in deriving the solvability condition. For this purpose, we introduce the following operators:

$$\mathcal{D}_0(\boldsymbol{x},\boldsymbol{\pi})=\bar{\alpha}^i(\boldsymbol{x})\pi_i+\beta\tilde{m}_D(\boldsymbol{x})\,, \tag{46}$$

$$\mathcal{D}(\boldsymbol{x},\boldsymbol{\pi})=\mathcal{D}_0(\boldsymbol{x},\boldsymbol{\pi})+\tilde{V}(\boldsymbol{x})\,. \tag{47}$$

The projection operator $\Pi_{\pm}$, such that $u_{0\pm}=\Pi_{\pm}u_0$ is hence defined as follows:

$$\Pi_{\pm}:=\frac{1}{2}\left[1\pm\frac{\mathcal{D}_0}{\lambda}\right]. \tag{48}$$

The properties listed below and proven in appendix, will allow us to derive a transport equation for u_0:

$$\Pi_\pm^2 = \Pi_\pm, \tag{49}$$
$$\Pi_\pm \Pi_\mp = 0, \tag{50}$$
$$\mathcal{D} = h_+ \Pi_+ + h_- \Pi_-, \tag{51}$$
$$\Pi_\pm \mathcal{D} = h_\pm \Pi_\pm, \tag{52}$$
$$\Pi_\pm \mathcal{D}_0 = \pm\lambda \Pi_\pm, \tag{53}$$
$$\Pi_\pm \bar{\alpha}^i(\boldsymbol{x}) \Pi_\pm = \omega_\pm^i \Pi_\pm, \tag{54}$$
$$\bar{\alpha}^i(\boldsymbol{x}) \Pi_\pm = \Pi_\mp \bar{\alpha}^i(\boldsymbol{x}) + \omega_\pm^i, \tag{55}$$

where $\omega_\pm^i = \pm\pi^i/\lambda$. In addition, it is Hermitian ($\Pi_\pm^\dagger = \Pi_\pm$). The solvability condition then becomes

$$u_{0\pm}^\dagger \Pi_\pm \left[\partial_t + \bar{\alpha}^i(\partial_i + \Omega_i)\right] \left(\Pi_\pm u_0^\pm\right) = 0, \tag{56}$$

where $p_i = \partial_i S^\pm(t,\boldsymbol{x})$ and thus $\pi_i = \partial_i S^\pm(t,\boldsymbol{x}) - \tilde{A}_i$. This is the basis to derive transport-like equations.

The first term in (56) is given by

$$T_1 := u_{0,\pm}^\dagger \Pi_\pm \frac{d}{dt}\left(\Pi_\pm u_{0,\pm}\right), \tag{57}$$
$$= u_{0,\pm}^\dagger \Pi_\pm \left(\frac{d}{dt}\Pi_\pm\right) u_{0,\pm} + u_{0,\pm}^\dagger \left(\frac{d}{dt} u_{0,\pm}\right). \tag{58}$$

The time-derivative is a total derivative. Since $\Pi_\pm$ depends explicitly on the momentum and position (not on time in our case). Denoting

$$F_i = \frac{d\pi_i}{dt},$$

we have

$$\frac{d\Pi_\pm}{dt} = \frac{\partial \Pi_\pm}{\partial \pi_i}\frac{d\pi_i}{dt} + \frac{d\Pi_\pm}{dx^i}\frac{dx^i}{dt} \tag{59}$$
$$= \frac{\partial \Pi_\pm}{\partial \pi_i} F_i + \frac{d\Pi_\pm}{dx^i}\omega_\pm^i. \tag{60}$$

On the right-hand-side, the derivatives can be evaluated as

$$\frac{\partial \Pi_\pm}{\partial \pi_i} = \pm\frac{1}{2}\frac{\partial}{\partial \pi_i}\left[\frac{\mathcal{D}_0}{\lambda}\right], \tag{61}$$
$$= \pm\frac{1}{2\lambda}\frac{\partial \mathcal{D}_0}{\partial \pi_i} \pm \frac{\mathcal{D}_0}{2}\frac{\partial}{\partial \pi_i}\left[\frac{1}{\lambda}\right], \tag{62}$$
$$= \pm\frac{\bar{\alpha}^i}{2\lambda} \mp \frac{\mathcal{D}_0}{2\lambda^2}\frac{\partial \lambda}{\partial \pi_i}, \tag{63}$$
$$= \pm\frac{\bar{\alpha}^i}{2\lambda} \mp \frac{\mathcal{D}_0}{4\lambda^3}\frac{\partial}{\partial \pi_i}\left(g^{jk}\pi_j\pi_k\right), \tag{64}$$

$$= \pm\frac{\bar{\alpha}^i}{2\lambda} \mp \frac{\mathcal{D}_0}{2\lambda^3}\pi^i\,, \tag{65}$$

$$= \pm\frac{\bar{\alpha}^i}{2\lambda} - \frac{\mathcal{D}_0}{2\lambda^2}\omega_\pm^i\,, \tag{66}$$

and

$$\frac{d\Pi_\pm}{dx^i} = \pm\frac{1}{2}\frac{d}{dx^i}\left[\frac{\mathcal{D}_0}{\lambda}\right], \tag{67}$$

$$= \pm\frac{1}{2\lambda}\frac{d\mathcal{D}_0}{dx^i} \pm \frac{\mathcal{D}_0}{2}\frac{d}{dx^i}\left[\frac{1}{\lambda}\right], \tag{68}$$

$$= \pm\frac{1}{2\lambda}\frac{d}{dx^i}\left[\bar{\alpha}^j\pi_j + \beta\tilde{m}_D\right] \mp \frac{\mathcal{D}_0}{2\lambda^2}\frac{d\lambda}{dx^i}\,, \tag{69}$$

$$= \pm\frac{1}{2\lambda}\left[\left(\partial_i\bar{\alpha}^j\right)\pi_j + \bar{\alpha}^j\left(\partial_i\pi_j\right) + \beta\left(\partial_i\tilde{m}_D\right)\right] \mp \frac{\mathcal{D}_0}{2\lambda^2}\frac{d\lambda}{dx^i}\,. \tag{70}$$

Using $\Pi_\pm\mathcal{D}_0 = \pm\lambda\Pi_\pm$ (from property 3) and property 4, the first term of T_1 becomes

$$T_{1,1} := u_{0,\pm}^\dagger\Pi_\pm\left(\frac{d}{dt}\Pi_\pm\right)u_{0,\pm}\,, \tag{71}$$

$$= u_{0,\pm}^\dagger\Pi_\pm\left[\frac{\partial\Pi_\pm}{\partial\pi_i}F_i + \frac{d\Pi_\pm}{dx^i}\omega_\pm^i\right]u_{0,\pm}\,, \tag{72}$$

$$= u_{0,\pm}^\dagger\Pi_\pm\left\{\left[\pm\frac{\bar{\alpha}^i}{2\lambda} - \frac{\mathcal{D}_0}{2\lambda^2}\omega_\pm^i\right]F_i\,,\right.$$

$$\left. + \left[\pm\frac{1}{2\lambda}\left[\left(\partial_i\bar{\alpha}^j\right)\pi_j + \bar{\alpha}^j\left(\partial_i\pi_j\right) + \beta\left(\partial_i\tilde{m}_D\right)\right] \mp \frac{\mathcal{D}_0}{2\lambda^2}\frac{d\lambda}{dx^i}\right]\omega_\pm^i\right\}u_{0,\pm}\,, \tag{73}$$

$$= \pm u_{0,\pm}^\dagger\Pi_\pm\frac{\omega_\pm^i}{2\lambda}\left[\left(\partial_i\bar{\alpha}^j\right)\pi_j + \omega_\pm^j\left(\partial_i\pi_j\right) + \beta\left(\partial_i\tilde{m}_D\right) \mp \frac{d\lambda}{dx^i}\right]u_{0,\pm}\,. \tag{74}$$

The second term in (56) is given by

$$T_2 := u_{0,\pm}^\dagger\Pi_\pm\bar{\alpha}^i\frac{d}{dx^i}\left(\Pi_\pm u_{0,\pm}\right), \tag{75}$$

$$= u_{0,\pm}^\dagger\Pi_\pm\bar{\alpha}^i\left[\frac{d\Pi_\pm}{dx^i}u_{0,\pm} + \Pi_\pm\partial_i u_{0,\pm}\right]. \tag{76}$$

The first term of T_2 can be written as

$$T_{2,1} := u_{0,\pm}^\dagger\Pi_\pm\bar{\alpha}^i\frac{d\Pi_\pm}{dx^i}\Pi_\pm u_{0,\pm}\,, \tag{77}$$

$$= u_{0,\pm}^\dagger\Pi_\pm\bar{\alpha}^i\left\{\pm\frac{1}{2\lambda}\left[\left(\partial_i\bar{\alpha}^j\right)\pi_j + \bar{\alpha}^j\left(\partial_i\pi_j\right) + \beta\left(\partial_i\tilde{m}_D\right)\right] \mp \frac{\mathcal{D}_0}{2\lambda^2}\frac{d\lambda}{dx^i}\right\}\Pi_\pm u_{0,\pm}\,, \tag{78}$$

$$= \pm u_{0,\pm}^\dagger\Pi_\pm\frac{\bar{\alpha}^i}{2\lambda}\left\{\left(\partial_i\bar{\alpha}^j\right)\pi_j + \bar{\alpha}^j\left(\partial_i\pi_j\right) + \beta\left(\partial_i\tilde{m}_D\right) \mp \frac{d\lambda}{dx^i}\right\}\Pi_\pm u_{0,\pm}\,, \tag{79}$$

$$= \pm u_{0,\pm}^\dagger\Pi_\pm\frac{1}{2\lambda}\left\{\bar{\alpha}^i\left(\partial_i\bar{\alpha}^j\right)\pi_j + \bar{\alpha}^i\bar{\alpha}^j\left(\partial_i\pi_j\right) + \bar{\alpha}^i\beta\left(\partial_i\tilde{m}_D\right) \mp \omega_\pm^i\frac{d\lambda}{dx^i}\right\}\Pi_\pm u_{0,\pm}\,. \tag{80}$$

while the second term is

$$T_{2,2} := u^{\dagger}_{0,\pm}\Pi_{\pm}\bar{\alpha}^i\Pi_{\pm}\partial_i u_{0,\pm}\,. \tag{81}$$

The third term in (56) is given by

$$T_3 := u^{\dagger}_{0,\pm}\Pi_{\pm}\bar{\alpha}^i\Omega_i\Pi_{\pm}u_{0,\pm}\,. \tag{82}$$

From the above calculations for T_1, T_2 and T_3, we deduce the transport equation:

$$\begin{aligned}
&u^{\dagger}_{0,\pm}\Pi_{\pm}\left[\partial_t+\omega^i_{\pm}\partial_i\right]u_{0,\pm}+u^{\dagger}_{0,\pm}\Pi_{\pm}\left\{\bar{\alpha}^i\Omega_i\right\}u_{0,\pm}\,,\\
&\pm u^{\dagger}_{0,\pm}\Pi_{\pm}\frac{1}{2\lambda}\left[\bar{\alpha}^i\left(\partial_i\bar{\alpha}^j\right)\pi_j+\bar{\alpha}^i\bar{\alpha}^j\left(\partial_i\pi_j\right)+\bar{\alpha}^i\beta\left(\partial_i\tilde{m}_D\right)\mp\omega^i_{\pm}\frac{d\lambda}{dx^i}\right]\Pi_{\pm}u_{0,\pm}\,,\\
&\pm u^{\dagger}_{0,\pm}\Pi_{\pm}\frac{1}{2\lambda}\left[\omega^i_{\pm}\left(\partial_i\bar{\alpha}^j\right)\pi_j+\omega^i_{\pm}\omega^j_{\pm}\left(\partial_i\pi_j\right)+\omega^i_{\pm}\beta\left(\partial_i\tilde{m}_D\right)\mp\omega^i_{\pm}\frac{d\lambda}{dx^i}\right]u_{0,\pm}=0\,,
\end{aligned} \tag{83}$$

or equivalently

$$\begin{aligned}
&u^{\dagger}_{0,\pm}\Pi_{\pm}\left[\partial_t+\omega^i_{\pm}\partial_i\right]u_{0,\pm}+u^{\dagger}_{0,\pm}\Pi_{\pm}\left\{\bar{\alpha}^i\Omega_i\right\}u_{0,\pm}\,,\\
&\quad\pm u^{\dagger}_{0,\pm}\Pi_{\pm}\frac{1}{2\lambda}\left\{\left(\bar{\alpha}^i+\omega^i_{\pm}\right)\left[\left(\partial_i\bar{\alpha}^j\right)\pi_j+\beta\left(\partial_i\tilde{m}_D\right)\right]\right.\\
&\quad\left.+\left(\bar{\alpha}^i\bar{\alpha}^j+\omega^i_{\pm}\omega^j_{\pm}\right)\left(\partial_i\pi_j\right)\mp 2\omega^i_{\pm}\frac{d\lambda}{dx^i}\right\}\Pi_{\pm}u_{0,\pm}=0\,.
\end{aligned} \tag{84}$$

To simplify this equation, we now evaluate the covariant derivative of $\omega^i_{\pm}$, starting from

$$\frac{d\omega^j_{\pm}}{dx^i}=\pm\frac{d}{dx^i}\left(\frac{\pi^j}{\lambda}\right), \tag{85}$$

$$=\pm\frac{1}{\lambda}\partial_i\pi^j\mp\frac{\pi^j}{\lambda^2}\frac{d\lambda}{dx^i}, \tag{86}$$

$$=\pm\frac{1}{\lambda}\partial_i\pi^j-\frac{\omega^j_{\pm}}{\lambda}\frac{d\lambda}{dx^i}, \tag{87}$$

$$=\pm\frac{1}{\lambda}\partial_i\left(g^{jl}\pi_l\right)-\frac{\omega^j_{\pm}}{\lambda}\frac{d\lambda}{dx^i}, \tag{88}$$

$$=\pm\frac{1}{\lambda}\left[\left(\partial_i g^{jl}\right)\pi_l+g^{jl}\left(\partial_i\pi_l\right)\right]-\frac{\omega^j_{\pm}}{\lambda}\frac{d\lambda}{dx^i}, \tag{89}$$

$$=\pm\frac{1}{\lambda}\left[-\left(\Gamma^j_{ik}g^{kl}+\Gamma^l_{ik}g^{jk}\right)\pi_l+g^{jl}\left(\partial_i\pi_l\right)\right]-\frac{\omega^j_{\pm}}{\lambda}\frac{d\lambda}{dx^i}, \tag{90}$$

$$=\pm\frac{1}{\lambda}\left[-\Gamma^j_{ik}\pi^k-\Gamma^l_{ik}g^{jk}\pi_l+g^{jl}\left(\partial_i\pi_l\right)\right]-\frac{\omega^j_{\pm}}{\lambda}\frac{d\lambda}{dx^i}, \tag{91}$$

$$=-\Gamma^j_{ik}\omega^k_{\pm}\pm\frac{1}{\lambda}\left[-\Gamma^l_{ik}g^{jk}\pi_l+g^{jl}\left(\partial_i\pi_l\right)\right]-\frac{\omega^j_{\pm}}{\lambda}\frac{d\lambda}{dx^i}\,. \tag{92}$$

Thus, the covariant derivative is given by

$$\nabla_i\omega^j_{\pm}:=\partial_i\omega^j_{\pm}+\Gamma^j_{ik}\omega^k_{\pm}\,, \tag{93}$$

$$=\pm\frac{1}{\lambda}\left[-\Gamma^l_{ik}g^{jk}\pi_l+g^{jl}\left(\partial_i\pi_l\right)\right]-\frac{\omega^j_{\pm}}{\lambda}\frac{d\lambda}{dx^i}\,. \tag{94}$$

The transport equation becomes

$$u_{0,\pm}^{\dagger}\Pi_{\pm}\left[\partial_t+\omega_{\pm}^i\partial_i\right]u_{0,\pm}+u_{0,\pm}^{\dagger}\Pi_{\pm}\left\{\bar{\alpha}^i\Omega_i\right\}u_{0,\pm}$$
$$+u_{0,\pm}^{\dagger}\Pi_{\pm}\left\{\pm\frac{1}{2\lambda}\left(\bar{\alpha}^i+\omega_{\pm}^i\right)\left[\left(\partial_i\bar{\alpha}^j\right)\pi_j+\beta\left(\partial_i\tilde{m}_D\right)\right]\right.$$
$$\left.\pm\frac{1}{2\lambda}\left(\bar{\alpha}^i\bar{\alpha}^j+\omega_{\pm}^i\omega_{\pm}^j\right)\left(\partial_i\pi_j\right)-\frac{\omega_{\pm}^i}{\lambda}\frac{d\lambda}{dx^i}\right\}\Pi_{\pm}u_{0,\pm}=0\,. \tag{95}$$

Using the expression for the covariant derivative, we get

$$u_{0,\pm}^{\dagger}\Pi_{\pm}\left[\partial_t+\omega_{\pm}^i\partial_i\right]u_{0,\pm}+u_{0,\pm}^{\dagger}\Pi_{\pm}\left\{\bar{\alpha}^i\Omega_i\right\}u_{0,\pm}$$
$$+u_{0,\pm}^{\dagger}\Pi_{\pm}\left\{\pm\frac{1}{2\lambda}\left(\bar{\alpha}^i+\omega_{\pm}^i\right)\left[\left(\partial_i\bar{\alpha}^j\right)\pi_j+\beta\left(\partial_i\tilde{m}_D\right)\right]\right.$$
$$\left.\pm\frac{1}{2\lambda}\left(\bar{\alpha}^i\bar{\alpha}^j+\omega_{\pm}^i\omega_{\pm}^j-2g^{ij}\right)\left(\partial_i\pi_j\right)+\nabla_i\omega_{\pm}^i\pm\frac{1}{\lambda}\Gamma_{ik}^l g^{jk}\pi_l\right\}\Pi_{\pm}u_{0,\pm}=0\,. \tag{96}$$

This concludes the proof. □

In flat space we recover the traditional result [56]:

Corollary 2.1. *In flat-space and with constant mass and no external field, the transport equation (95) degenerates into*

$$u_{0,\pm}^{\dagger}\Pi_{\pm}\left[\partial_t+\omega_{\pm}^i\partial_i\right]u_{0,\pm}=0\,. \tag{97}$$

3. Applications to strained graphene

In this section, we study some properties of the classical model used in the framework of strained graphene. The dynamics of electron on graphene surfaces can be modeled by a massless Dirac equation, derived from the low energy limit of tight-binding models (expansion of the dispersion relation about Dirac points), see [5, 51]. The corresponding Dirac equation on strained graphene surfaces typically reads as (12) where

- $\tilde{m}_D\equiv 0$ (massless Dirac equation) and $\tilde{V}\equiv 0$.
- In presence of in-plane deformation of a lattice of carbon atoms, the function $\tilde{A}_i$ refers to a *pseudomagnetic field* (mimicking an external field), the function $\tilde{\Omega}$ corresponds to the *spin-affine connection*, and $\bar{\alpha}_i$ is a space-dependent function.

It is also assumed that the graphene has a perfect crystal structure (no dislocations nor defects), an infinite extent (no edge effects) and no interaction with external degrees of freedom like phonons. We also neglect any carrier-carrier interactions via the Coulomb force. We again refer to [5, 51] for details.

We will present some numerical experiments illustrating those properties, as well as some comparisons with a standard tight-binding model from which the Dirac equation is derived. We report the solutions to the corresponding equation in *curved space*. As we consider here, small scale deformations the corresponding solutions in Cartesian coordinates are close. The latter provides a more accurate description of the dynamics but with a much higher computational

cost. From (36) and (42), the model is explicitly rewritten in the following form

$$\frac{dx}{dt} = \pm v_D \frac{\pi^x(t,\boldsymbol{x})}{|\boldsymbol{\pi}(\boldsymbol{x})|}, \tag{98}$$

$$\frac{dy}{dt} = \pm v_D \frac{\pi^y(t,\boldsymbol{x})}{|\boldsymbol{\pi}(\boldsymbol{x})|}, \tag{99}$$

$$\frac{d\pi_x}{dt} = F_x^{\text{geom}} + F_x^{\text{lorentz}}, \tag{100}$$

$$\frac{d\pi_y}{dt} = F_y^{\text{geom}} + F_y^{\text{lorentz}}, \tag{101}$$

where the force due to the geometrical deformation explicitly reads

$$\begin{aligned} F_x^{\text{geom}} &= \Gamma_{xx}^x(\boldsymbol{x})\pi_x(\boldsymbol{x})\frac{dx}{dt} + \Gamma_{xy}^x(\boldsymbol{x})\pi_x(\boldsymbol{x})\frac{dy}{dt} \\ &\quad + \Gamma_{xx}^y(\boldsymbol{x})\pi_x(\boldsymbol{x})\frac{dx}{dt} + \Gamma_{xy}^y(\boldsymbol{x})\pi_x(\boldsymbol{x})\frac{dy}{dt}, \\ F_y^{\text{geom}} &= \Gamma_{yx}^x(\boldsymbol{x})\pi_x(\boldsymbol{x})\frac{dx}{dt} + \Gamma_{yy}^x(\boldsymbol{x})\pi_x(\boldsymbol{x})\frac{dy}{dt} \\ &\quad + \Gamma_{yx}^y(\boldsymbol{x})\pi_x(\boldsymbol{x})\frac{dx}{dt} + \Gamma_{yy}^y(\boldsymbol{x})\pi_x(\boldsymbol{x})\frac{dy}{dt}. \end{aligned} \tag{102}$$

In the following, we rewrite the classical model in term of displacement fields as proposed in [51]. More specifically, we define the forces using dispacement fields in the z-direction (resp. in the (x,y)-plane) defined by a smooth function h (resp. $u(x,y)$). Then the classical model can be rewritten as

$$\begin{aligned} F_x^{\text{Lorentz}} &= -\frac{\beta}{2a_{\text{cc}}}\left(\partial_x\varepsilon_{xx} - \partial_x\varepsilon_{yy} - 2\partial_y\varepsilon_{xy}\right)\dot{y}, \\ F_x^{\text{Lorentz}} &= \frac{\beta}{2a_{\text{cc}}}\left(\partial_y\varepsilon_{xx} - \partial_y\varepsilon_{yy} - 2\partial_x\varepsilon_{xy}\right)\dot{x}, \end{aligned}$$

where a_{cc} the atom-atom distance in pristine graphene, β is the Grünensen parameter [51], and where

$$\begin{aligned} \varepsilon_{xx}(\boldsymbol{x}) &= \partial_x u_x(\boldsymbol{x}) + \frac{1}{2}\partial_x h(\boldsymbol{x})^2, \\ \varepsilon_{xy}(\boldsymbol{x}) &= \frac{1}{2}\left(\partial_y u_x(\boldsymbol{x}) + \partial_x u_y(\boldsymbol{x})\right) + \frac{1}{2}\partial_x h(\boldsymbol{x})\,\partial_y h(\boldsymbol{x}), \\ \varepsilon_{yy}(\boldsymbol{x}) &= \partial_y u_y(\boldsymbol{x}) + \frac{1}{2}\partial_y h(\boldsymbol{x})^2. \end{aligned} \tag{103}$$

In the following, we consider some relatively general strained graphene configurations.

In- and Out-of-plane deformation. We are here interested in numerical experiments for in- and out-of-plane deformations. More specifically, we assume that

$$\begin{aligned} u_x(x,y) &= 0, \\ u_y(x,y) &= a_0 y, \\ h(x,y) &= h_0 \exp\left(-R_x(x-x_c)^2 - R_y(y-y_c)^2\right). \end{aligned}$$

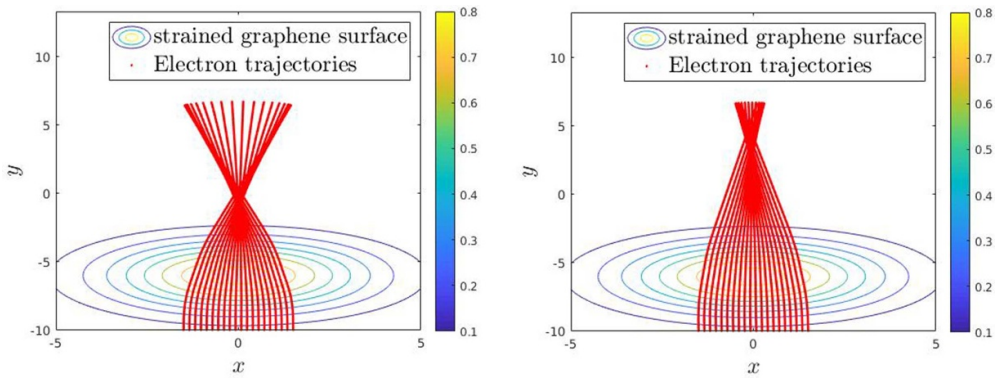

Figure 1. 20 classical trajectories on strained graphene surface. (Left) $a_0 = 0$. (Right) $a_0 = 0.35$.

with $h_0 = 0.85$, $x_c = -6$, $y_c = 0$, $v_D = 1$ and $R_x = 2/25$, $R_y = 4/25$. We assume that the final time is $T = 12.5$ and the physical domain is $[-10,10] \times [-5,5]$ in nm. The physical parameters are $\beta = 3.37$,$a_{cc} = 14.2$ Angstrom. We consider 20 electron trajectories with initial positions between $x_0 \in [-3/2, 3/2]$ and $y_0 = 0$, and the initial velocity set to $(5,0)$. We report the trajectories in figure 1 with $a_0 = 0$ (Left) and with $a_0 = 0.35$ (Right). A focusing effect due to the deformation of the surface is observed figure 1(Left), with a focal point behind the top of the Gaussian. The distance to the focal point is increased by the strain in the y-direction, as shown in figure 1(Right).

From the trajectories, it is also possible to reconstruct an approximate wavefunction ψ_{approx} at any time t. More specifically, we consider an initial wavefunction $\phi_0(x,y)$. Hence, at any (t,x,y), if there exists a trajectory $(x_{x_0}(t), y_{y_0}(t))$ such that i) $(x(0),y(0)) = (x_0,y_0)$ and $x,y = (x_{x_0}(t), y_{y_0}(t))$, then:

$$|\psi_{\text{approx}}(t,x,y)| = \phi_0(x_0,y_0)\,. \tag{104}$$

It is also possible to include the contribution of the phase $\exp\left(\mathtt{i}S^{\pm}(t,x,y)/\varepsilon\right)$. The latter can be obtained from

$$\partial_t S^{\pm}(t,\boldsymbol{x}) = S^{\pm}(0,\boldsymbol{x}) \mp v_D \int_0^t |\boldsymbol{\pi}(s)|ds\,.$$

For instance, let us report in figure 2, the graph of $|\psi_{\text{approx}}|$ at different times, and reconstructed from the trajectories with $a_0 = 0$, $u_x = u_y = 0$, and with

$$\phi_0(x,y) = \exp\left(-\left(x^2 + (y+10)^2\right)/2\right)\,.$$

We report in figure 2 the solutions at time $t = 0$, $t = 5$, $t = 10$, $t = 12.5$ from 2500 trajectories using (104). Close and after the focus, the reconstruction of the wavefunction is not elementary anymore as the trajectories are crossing each other. This can also induce the well-known problem of caustics where the semi-classical approximation breaks down.

Qualitative comparison with tight-binding model. We here propose a qualitative comparison between the classical model presented in this paper and a standard tight-binding model

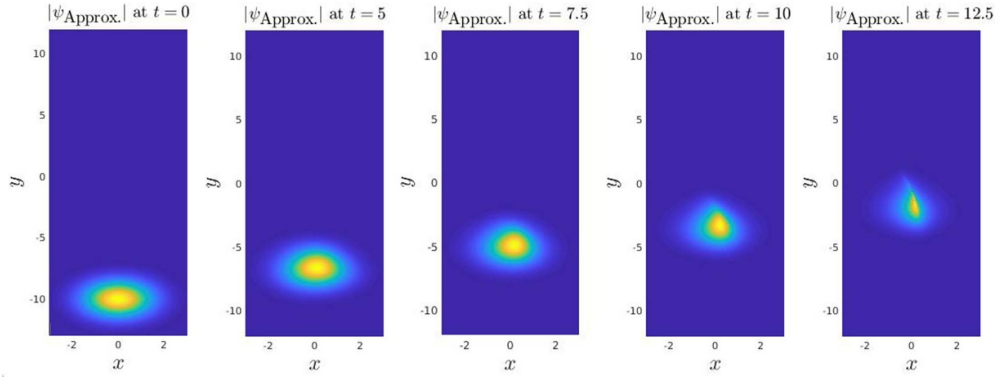

Figure 2. $(x,y) \Rightarrow |\psi_{\text{approx}}(t,x,y)|$. From left to right $t=0$,5, 7.5, 10, 12.5.

for strained graphene [5, 47, 58–61]. We recall that from the tight-binding model, a Dirac equation can be derived in the low energy limit (in the vicinity of the so-called Dirac point); from the latter model, we have derived in this paper a (semi-)classical model describing electron trajectories. A rigorous quantitative comparison would require very fine investigation and will be proposed in a forthcoming paper, including in particular a rigorous comparison with a Dirac model. The simulations proposed below are performed using the libraries `pybinding` and `kwant`. We refer to [62, 63] for details.

The chosen surface is parameterized as follows: $h(x,y) = h_0 \exp\big(-R_x(x-x_c)^2 - R_y(y-y_c)^2\big)$ with $x_c = 6$, $y_c = 0$, $h_0 = 0.85$, $R_x = 2/25$, $R_y = 4/25$. We first assume that there is no straining in the x,y-directions ($u_x = u_y = 0$). The hopping is defined as

$$t(x,y) = t_0 \exp\left(-\beta\left(\ell(x,y,z)/a_{\text{cc}} - 1\right)\right),$$

where t_0 is the hopping energy for pristine graphene, $\beta = 3.37$ controls the strength of the hopping modulation and ℓ is the distance between two atoms with $a_{\text{cc}} = 1.42$ Angstrom. The physical domain is $[-20,20]\times[-15,15]$ and the initial wavefunction is a Gaussian function centered at $(-6,0)$ is of the form $\psi_0(x,y) = \exp\big(-(x+10)^2/9 - y^2/9\big)\exp(\mathrm{i}y)$. The final computational time is $T = 25$. We report in figure 3 the wavefunction at time $t = 5,10,15,20,25$ showing the focusing effect occuring for the deformed surface, which is qualitatively similar to the ones obtained with the classical model, at least before and right after the focusing. We perform the same test when the graphene surface is strained in the y-direction (as in the classical case) with a deformation $u_y(x,y) = 0.35y$ and $R_x = 2/25$, $R_y = 4/25$, see figure 5. We display in figure 4, hexagonal cells (Left), the full domain (Middle) without strain, and the hexagonal cell with strain in y-direction.

We observe that the wavefunction is focused in both cases as it was observed in the classical models. When the width of the Gaussian is increased, we also observe a splitting of the wavefunction.

4. Applications to edge states dynamics in photonic graphene

The semi-classical analysis developed in section 2 is applied here to the evolution of edge states in photonic graphene. This topological material, made of an array of coupled waveguides arranged in a honeycomb configuration, share many properties with graphene. In particular,

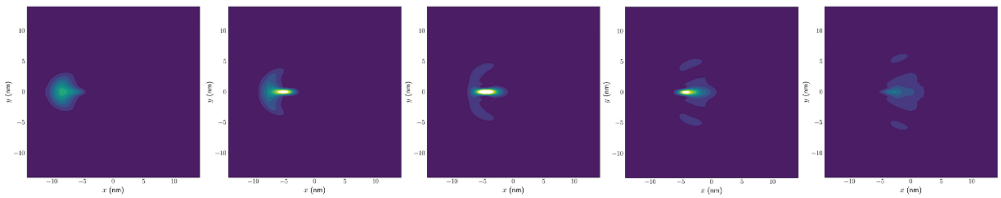

Figure 3. Without strain in x, y-directions. From left to right: tight-binding wavefunction at $t = 5$, $t = 10$, $t = 15$, $t = 20$, $t = 25$.

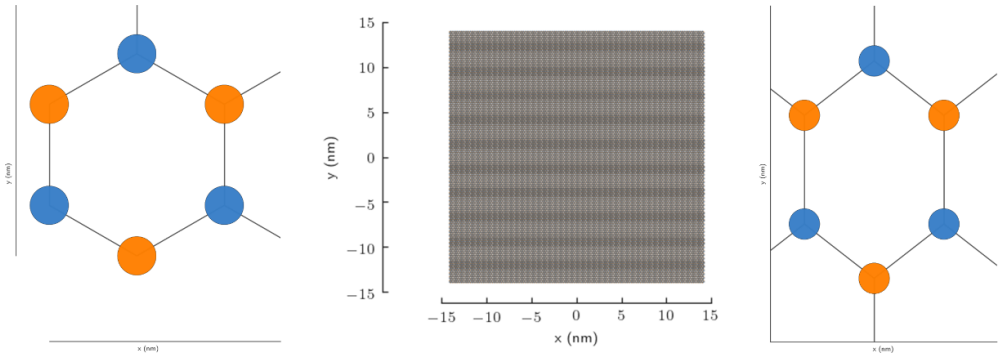

Figure 4. (Left) Hexagonal cell (no strain), (Middle) Hexagonal cell with strain in y-direction.

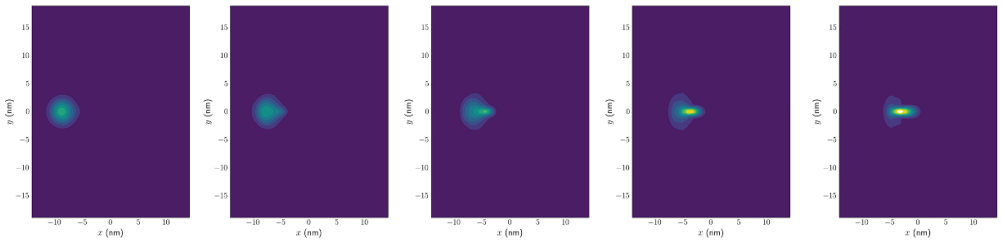

Figure 5. With strain in x, y-directions. From left to right: tight-binding wavefunction at $t = 5$, $t = 10$, $t = 15$, $t = 20$, $t = 25$.

light propagation in these complex structures is characterized by the presence of Dirac points at low energy. The dynamics of photonic graphene edge states in a slowly modulated honeycomb media can be described by a Dirac equation with a space-dependent mass-term [53] in the form of equation (11). We are specifically interested in the dynamics of edge states along domain-walls which breaks the CP-symmetry of photonic graphene (see [53, 64]). Physically, these systems are reminiscent of Dirac materials with line-defects and one of their main properties is the existence of robust quantum states close to the edge. In this section, the latter will be explored dynamically using the semi-classical formalism developed in previous sections.

4.1. A classical model for photonic graphene

In the following, we consider the classical model (corresponding to LO in ε) for photonic graphene (an optical analogue to graphene) in *flat space*, where the space-dependent mass term m models a wall-function/interface accounting for a line-defect between two domains. The Dirac equation modeling the dynamics of edge states in photonic graphene is derived from Maxwell's equations (rewritten in the form a Schrödinger equation with periodic coefficients) on a hexagonal lattice. As proven in [53], in its low energy limit it degenerates into a Dirac-like equation (12) such that

- $\tilde{m}_D$ as a positive function.
- $\tilde{V} \equiv 0$.
- $\tilde{A}_i \equiv 0$.
- $\bar{\alpha}_i \equiv \alpha_i$ are constant and correspond to the standard Pauli's matrices.

In this case, based on theorem 2.1 and setting $m = m_D$ and $\boldsymbol{\pi} = \boldsymbol{p}$, the system of equations for the classical modelling of edge states is reduced to:

$$\begin{aligned} \frac{d\boldsymbol{x}}{dt} &= v_D \frac{\boldsymbol{p}}{\sqrt{\boldsymbol{p}^2 + m^2(\boldsymbol{x})\, v_D^2}}, \\ \frac{d\boldsymbol{p}}{dt} &= -\frac{v_D^3}{2\sqrt{\boldsymbol{p}^2 + m^2(\boldsymbol{x})\, v_D^2}} \nabla_{\boldsymbol{x}} m^2(\boldsymbol{x}). \end{aligned} \tag{105}$$

The objective of this section is to study the propagation of edge states described semi-classically by (105). The interest of using this model is i) its simplicity, and ii) its ability to consider in parallel a very large number of trajectories to model the wave propagation.

We assume that the material under consideration is a photonic graphene sheet with a 2D domain Ω, large enough to avoid boundary effects. The domain is separated in two subdomains by an interface parameterized by $x_2 = f(x_1)$ where f is a smooth function. From this parameterization of the interface it is possible to define a mass-term. Following [65], we use an interface-function given by

$$m(\boldsymbol{x}) = \tanh\left(\nu\left(f(x_1) - x_2\right)\right), \tag{106}$$

where ν is a large parameters which characterizes the sharp transition between the 2 regions. The interface-function is displayed in figure 6 with $f(x) = 0.2\cos(x)$.

4.2. Analysis

This section is dedicated to the analysis of the classical model (105). The following proposition shows its relative accuracy.

Proposition 4.1. *Assuming that f is not an affine function, then for any $(\boldsymbol{x}_0, \boldsymbol{p}_0) \in \Omega \backslash \mathcal{I} \times \mathbb{R}^2$, the solution $(\boldsymbol{x}, \boldsymbol{p})$ to (105) is such that the function $t \mapsto x_2(t) - f(x_1(t))$ does not converge to 0, when t goes to infinity.*

In other words, according to (105), the edge states never follow the interface exactly, even asymptotically at large times. Rather, they are oscillating around the interface with a bounded amplitude (demonstrated in proposition 4.2 and numerically). Hereafter, these solutions to (105) will be referred as quasi-edge states.

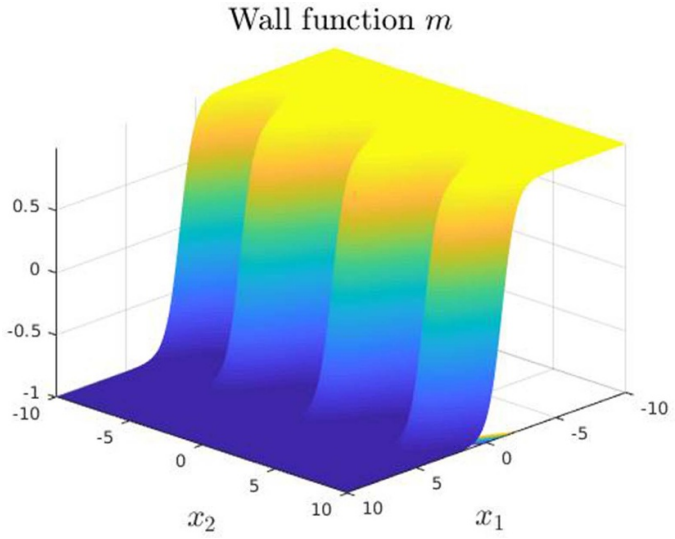

Figure 6. Graph of the interface-function $m(\boldsymbol{x})$, $\boldsymbol{x} \in \mathbb{R}^2$.

Proof. The proof of proposition 4.1 is straightforward. Indeed assuming $x_2(t) - f(x_1(t)) = 0$ (for some $t > 0$), implies that i) $m(\boldsymbol{x}(t)) = 0$, so that $\dot{\boldsymbol{p}}(t) = \boldsymbol{0}$ and $\dot{\boldsymbol{x}}(t) = \boldsymbol{0}$ and ii) $\dot{x}_2(t) = \dot{x}_1 f'(x_1(t))$. In this case, for any $t > 0$

$$(\boldsymbol{x}(t), \boldsymbol{p}(t)) = \left(\boldsymbol{x}(0) + \nu \frac{\boldsymbol{p}(0)}{|\boldsymbol{p}(0)|} t, \boldsymbol{p}(0)\right) \in \mathcal{I}.$$

If $\boldsymbol{x}(t) \in \mathcal{I}$, then

$$x_2(0) + \frac{p_2(0)}{|\boldsymbol{p}(0)|}\nu t = f\left(x_1(0) + \frac{p_1(0)}{|\boldsymbol{p}(0)|}\nu t\right).$$

In particular, as $\dot{x}_2(t) = \dot{x}_1 f'(x_1(t))$ for any $t > 0$, we get

$$\frac{p_2(0)}{|\boldsymbol{p}(0)|}\nu = f'\left(x_1(0) + \frac{p_1(0)}{|\boldsymbol{p}(0)|}\nu t\right)\frac{p_1(0)}{|\boldsymbol{p}(0)|}\nu.$$

That is, for any $t > 0$

$$f'\left(x_1(0) + \frac{p_1(0)}{|\boldsymbol{p}(0)|}\nu t\right) = \frac{p_2(0)}{p_1(0)}.$$

This implies that f' is a constant function, more specifically given by $f(x) = x p_2(0)/p_1(0)$. □

In the following, it will be useful to introduce the function $\epsilon := f(x_1) - x_2$, so that (105) can be rewritten as follows

$$\begin{aligned}
\dot{x}_1 &= \frac{p_1 \nu}{\sqrt{\boldsymbol{p}^2 + m^2(\boldsymbol{x})\nu^2}}, \\
\dot{\epsilon} &= \nu \frac{p_1 f'(x_1) - p_2}{\sqrt{\boldsymbol{p}^2 + m^2(\epsilon)\nu^2}}, \\
\dot{p}_1 &= \nu^4 \frac{f'(x_1)\, m(\epsilon)\left(1 - m^2(\epsilon)\right)}{\sqrt{\boldsymbol{p}^2 + m^2(\boldsymbol{x})\nu^2}}, \\
\dot{p}_2 &= -\nu^4 \frac{m(\epsilon)\left(1 - m^2(\epsilon)\right)}{\sqrt{\boldsymbol{p}^2 + m^2(\boldsymbol{x})\nu^2}}.
\end{aligned} \tag{107}$$

Notice in particular that $\dot{p}_1(t) + f'(x_1(t))\dot{p}_2(t) = 0$ for all t, with initial condition $(x_{10}, \epsilon_0, p_{10}, p_{20})$ such that $x_{20} = f(x_{10}) - \epsilon_0$.

As proven above, ϵ can be small but not zero. Hereafter, we will hence also assume that $\nu m(\epsilon)$ is large, for ν large. For the sake of simplicity, we will also assume in the following proposition that the interface is flat, and more specifically $f'(x) = 1$. We then show that the trajectory of the quasi edge-state is oscillatory, at least for small times. Using continuity arguments, we deduce that this result remains true from non-flat smooth interfaces.

Proposition 4.2. *We assume that i) $f'(x) = 1$ and that ii) initially the solution to (107) is close enough to the interface. For ν large enough, the solution to (107) is oscillatory about the interface, at least for t small enough.*

Proof. First let us rewrite (105), as follows

$$\begin{aligned}
\dot{x}_1 &= \frac{p_1 \nu}{\sqrt{\boldsymbol{p}^2 + m^2(\boldsymbol{x})\nu^2}}, \\
\dot{\epsilon} &= \nu \frac{p_1 - p_2}{\sqrt{\boldsymbol{p}^2 + m^2(\epsilon)\nu^2}}, \\
\dot{p}_1 &= \nu^4 \frac{m(\epsilon)\left(1 - m^2(\epsilon)\right)}{\sqrt{\boldsymbol{p}^2 + m^2(\boldsymbol{x})\nu^2}}, \\
\dot{p}_2 &= -\nu^4 \frac{m(\epsilon)\left(1 - m^2(\epsilon)\right)}{\sqrt{\boldsymbol{p}^2 + m^2(\boldsymbol{x})\nu^2}}.
\end{aligned} \tag{108}$$

Notice in particular that $\dot{p}_1(t) + \dot{p}_2(t) = 0$ for all $t > 0$ with initial condition is denoted $(x_{10}, \epsilon_0, p_{10}, p_{20})$, with in particular $x_{20} = f(x_{10}) - \epsilon_0$. Let us now introduce a new variable $\boldsymbol{Y} = (x_1, \epsilon, p_1, p_2)^T$ and a function $\mathcal{H}$ such that

$$\mathcal{H}(\epsilon, \boldsymbol{p}, \nu) := \frac{\nu}{\sqrt{\boldsymbol{p}^2 + m^2(\epsilon)\nu^2}}.$$

We get for ν large, $m(\epsilon) \sim_{\nu\to+\infty} \pm\left(1-e^{-2\epsilon\nu}\right)$. For $\boldsymbol{p}^2$ negligible compared to $m^2\nu^2$, which is a reasonable assumption for $m\nu$ large, we get

$$\begin{aligned}
\frac{p_1\nu}{\sqrt{\boldsymbol{p}^2+m^2(\epsilon)(\boldsymbol{x})\nu^2}} &\sim_{\nu\to+\infty} \frac{p_1}{\sqrt{m^2(\epsilon)}}\,,\\
\nu\frac{p_1-p_2}{\sqrt{\boldsymbol{p}^2+m^2(\epsilon)\nu^2}} &\sim_{\nu\to+\infty} \frac{p_1-p_2}{\sqrt{m^2(\epsilon)}}\,,\\
\nu^4\frac{m(\epsilon)\left(1-m^2(\epsilon)\right)}{\sqrt{\boldsymbol{p}^2+m^2(\epsilon)(\boldsymbol{x})\nu^2}} &\sim_{\nu\to+\infty} \nu^3\frac{m(\epsilon)\left(1-m^2(\epsilon)\right)}{\sqrt{m^2(\epsilon)}}\,,\\
-\nu^4\frac{m(\epsilon)\left(1-m^2(\epsilon)\right)}{\sqrt{\boldsymbol{p}^2+m^2(\epsilon)(\boldsymbol{x})\nu^2}} &\sim_{\nu\to+\infty} -\nu^3\frac{m(\epsilon)\left(1-m^2(\epsilon)\right)}{\sqrt{m^2(\epsilon)}}\,.
\end{aligned}$$

We then consider the following system $\dot{\boldsymbol{Z}} = G(\boldsymbol{Z})$, where $\boldsymbol{Z} = (z_1, e, q_1, q_2)^T$ and

$$\begin{aligned}
G(\boldsymbol{Z}) = \Bigg(& q_1/\sqrt{m^2(\epsilon)}, (q_1-q_2)/\sqrt{m^2(\epsilon)}\,,\\
& -\nu^3 m(\epsilon)\left(1-m^2(\epsilon)\right)/\sqrt{m^2(\epsilon)}\,,\\
& \nu^3 m(\epsilon)\left(1-m^2(\epsilon)\right)/\sqrt{m^2(\epsilon)}\Bigg)^T\,.
\end{aligned} \tag{109}$$

Let us consider the following initial condition: $\boldsymbol{Z}(0) = (x_{10}, \epsilon_0, p_{10}, p_{20})^T$ with $\epsilon_0 = f(x_{10}) - x_{20}$, non-zero. We intend to prove that the solution to (109) has an oscillatory behavior. For this purpose, we compute

$$\begin{aligned}
\ddot{q}_2 &= -2\nu^4\frac{m^4(\epsilon)-m^2(\epsilon)\dot{e}}{\left(m^2(\epsilon)\right)^{3/2}}\,,\\
&= 2\nu^4\left(m^2(\epsilon)-1\right)q_2\,,
\end{aligned} \tag{110}$$

where we have used that $\dot{q}_1 = -\dot{q}_2$ and $\dot{\epsilon} = (q_1-q_2)/\sqrt{m^2(\epsilon)}$. Using that $m(\epsilon) < 1$ close to the interface (see (106)), we deduce that the coefficient in front q_2 on the right hand side of (110) is negative for all t, which implies that the solution is oscillatory. The same argument naturally applies for q_1. Moreover, as $\dot{z}_1 = p_1/\sqrt{m^2(\epsilon)}$ with $m^2(\epsilon)$ non-zero, we also deduce that at least for short times, z_1 is also oscillatory, as well as ε.

Next, we set $\boldsymbol{W} := \boldsymbol{Y} - \boldsymbol{Z}$ with $\boldsymbol{W}(0) = \boldsymbol{0}$. Formally $\dot{\boldsymbol{W}} = F(\boldsymbol{Y}) - G(\boldsymbol{Z})$. For ν large $F(\boldsymbol{Y}) \sim_{\nu\to+\infty} G(\boldsymbol{Y}) + H(\boldsymbol{Y})$. As

$$\frac{1}{\sqrt{\boldsymbol{p}^2+m^2\nu^2}} - \frac{1}{\sqrt{m^2\nu^2}} = -\frac{\boldsymbol{p}}{m^2\nu^2} + O\left(\nu^{-4}\right)\,,$$

we deduce that $H(\boldsymbol{X}) = O(G(\boldsymbol{X})\nu^{-2})$. Then for some $\boldsymbol{\xi}$, we have

$$\begin{aligned}
\dot{\boldsymbol{W}} &= G(\boldsymbol{Y}) - G(\boldsymbol{Z}) + H(\boldsymbol{X})\\
&= \nabla G(\boldsymbol{\xi})\,\boldsymbol{W} + H(\boldsymbol{W})\,.
\end{aligned}$$

with $\boldsymbol{W}(0) = \boldsymbol{0}$ and $\|\nabla G\|_\infty \leqslant M$ for some finite number $M > 0$; there also exists $\upsilon > 0$ small for ν large, such that $\|H\|_\infty \leqslant \upsilon$. We conclude from Grönwall, that for ν large, the trajectory to the full system are close to those of the simplified one which were proven to be oscillatory, at least for small times. □

4.3. Numerical experiments

We propose a set of numerical experiments to illustrate the above analysis. To solve the set of equations of motion, we use the second order Störmer-Verlet symplectic scheme [66].

Experiment 0. *Flat interface*. In this first experiment, we are interested in illustrating propositions 4.1 and 4.2 by taking $f(x_1) = x_1$. We consider the initial data $(x_{10}, x_{20}, p_{10}, p_{20}) = (0,0,0,1)$ and $\nu = 10$. We report in figure 7(Top), the corresponding trajectory of the edge state along the interface $\{(x_1(t), x_2(t)),\ t \in [0,T]\}$ with $T = \pi/32$ as $\boldsymbol{x}(0) \in \mathcal{I}$. We also report in figure 7(Bottom) the first component of the momentum $t \mapsto p_1(t)$ for $t \in [0,T]$. On the same graph we report a trajectory if initially $\boldsymbol{x}(0) \notin \mathcal{I}$, $(x_{10}, x_{20}, p_{10}, p_{20}) = (0, -0.1, 0, 1)$. In this case, we see that the edge state trajectory does not converge to the interface but oscillates about it, as expected from proposition 4.2.

Experiment 1. *Sinusoidal interface*. We propose the following experiment $f(x_1) = \alpha\cos(x_1)$ with $\alpha = 0.2$. We consider the initial data $(x_{10}, x_{20}, p_{10}, p_{20}) = (-0.1, 0, 1, 0.1)$ and $\nu = 10$. We report in figure 8(Top) the corresponding trajectory of the quasi-edge state oscillating along the interface $\{(x_1(t), x_2(t)),\ t \in [0,T]\}$ with $T = \pi$. We also report in figure 8(Middle) $t \mapsto \epsilon(t)$ and the momentum $t \mapsto \boldsymbol{p}(t)$. As expected the trajectory again does not converge to the interface and oscillates about it.

Experiment 2. The phase of the oscillatory solution to (107) is dependent on the initial condition, it is natural to compute the average of many classical trajectories to model a quantum trajectory; it is expected that an average process will be more accurate to model edge states close to the interface. To verify this, we propose the following experiment. We consider a sequence of initial data: $(\boldsymbol{x}_0^{(k)}, \boldsymbol{p}_0) := (x_1^{(k)}(0), x_2(0), p_1(0), p_2(0))$, where $k \in \{1, \cdots, K\}$, for some large integer K, where $x_1^{(k)}(0) = (k-1)/32$, $y_0 = -0.1$, $p_1(0) = p_2(0) = 1$. We denote by $(x_1^{(k)}, \epsilon^k, p_1^{(k)}, p_2^{(k)})$ the corresponding solution to (107), and we compute

$$x_{1;K} = \frac{1}{K}\sum_{k=1}^{K} x_1^{(k)},\ \epsilon_K = \frac{1}{K}\sum_{k=1}^{K} \epsilon^{(k)}.$$

We then report in figure 9, the average quasi-edge state trajectories $t \mapsto \epsilon_K(t)$, for $K = 1, 4, 16, 1024, 4096$ and $T = \pi/16$. This test shows that the average over many trajectories can provide a good estimate of edge state dynamics.

All the numerical experiments are consistent with propositions 4.1 and 4.2. They demonstrate clearly the oscillating behaviour of edge states around the domain wall interface. This property is reminiscent of a waveguide, allowing for effective transmission of waves along the line-defect between the two domains.

5. Conclusion

In this article, the semi-classical approximation for Dirac materials described by the Dirac equation in curved space-time was obtained to zeroth and first order. Compared to the case in flat space, a geometric force appears in the classical equations of motion. This force can have a significant effect on electron dynamics, as was demonstrated using specific examples in strained graphene. We also demonstrated that the spin dynamics is governed by a transport-like equation when the second order approximation is taken into account. This part of our formalism was not studied numerically, but this will be the topic of future investigations. The

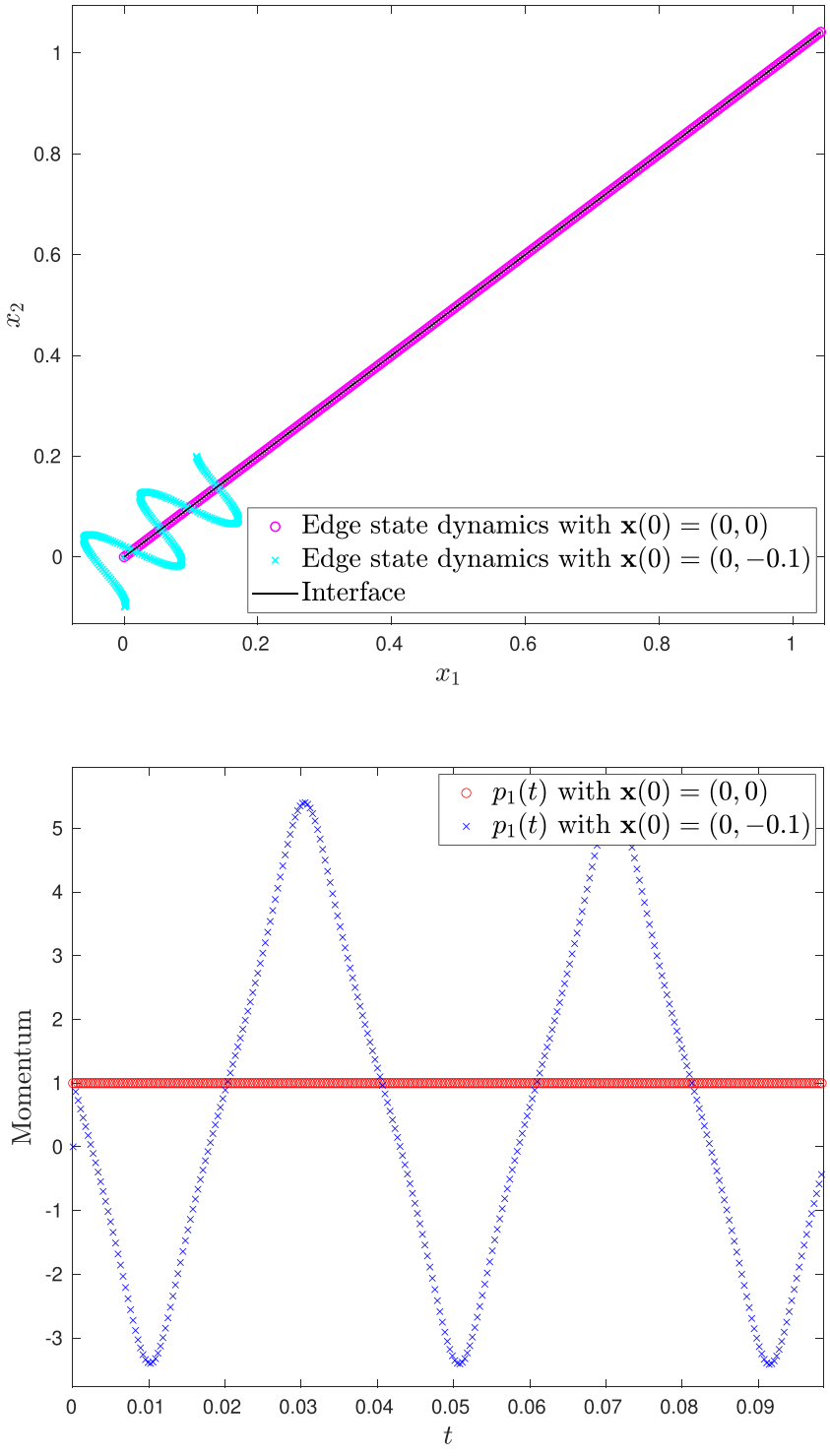

Figure 7. Experiment 0. (Top) Trajectory $\{(x_1(t), x_2(t)),\, t \in [0,T]\}$. (Bottom) First component of momentum $t \mapsto p_1(t)$.

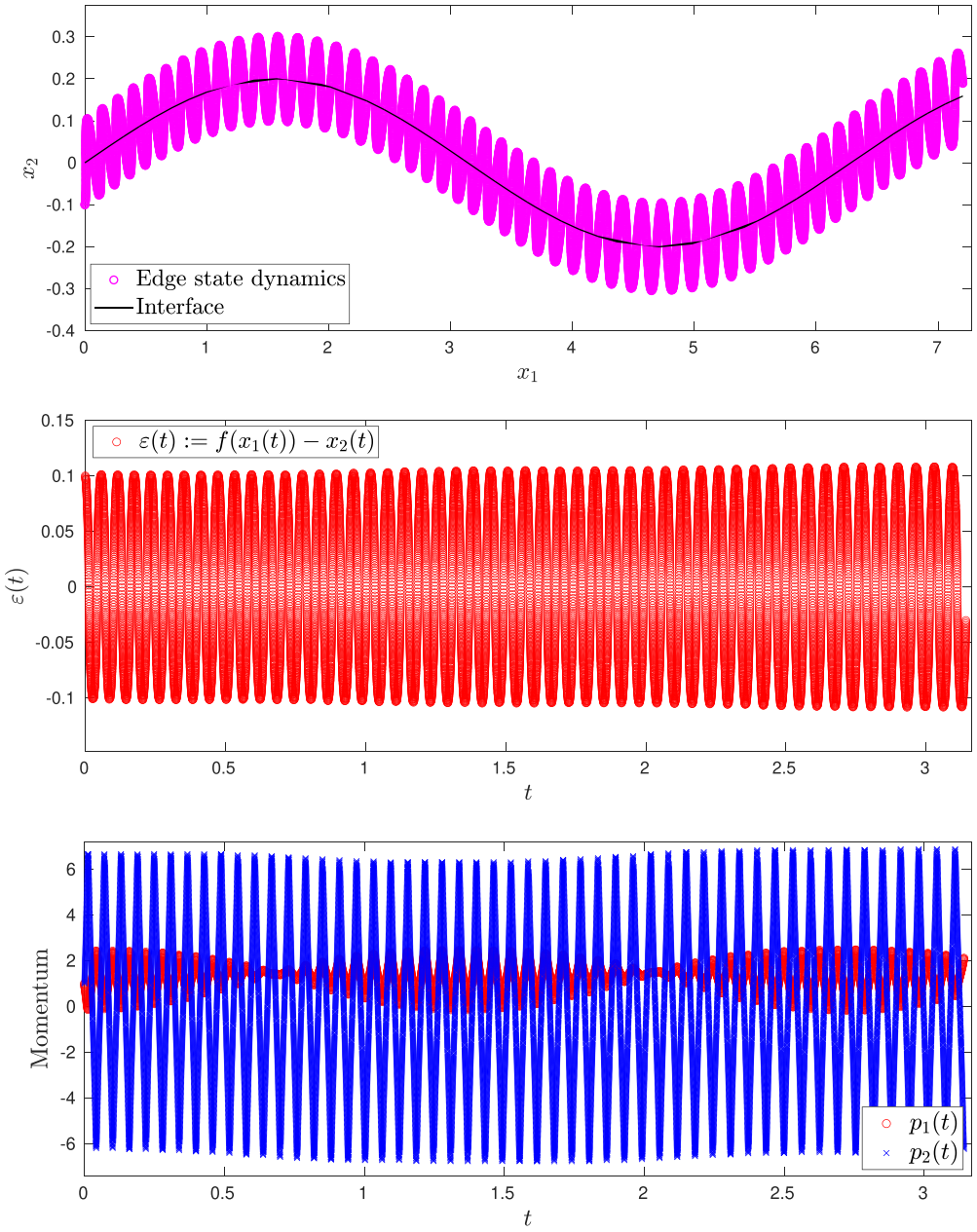

Figure 8. Experiment 1. (Top) Trajectory $\{(x_1(t), x_2(t)),\ t \in [0,T]\}$. (Middle) $t \mapsto \epsilon(t)$. (Bottom) Momentum $t \mapsto \boldsymbol{p}(t)$.

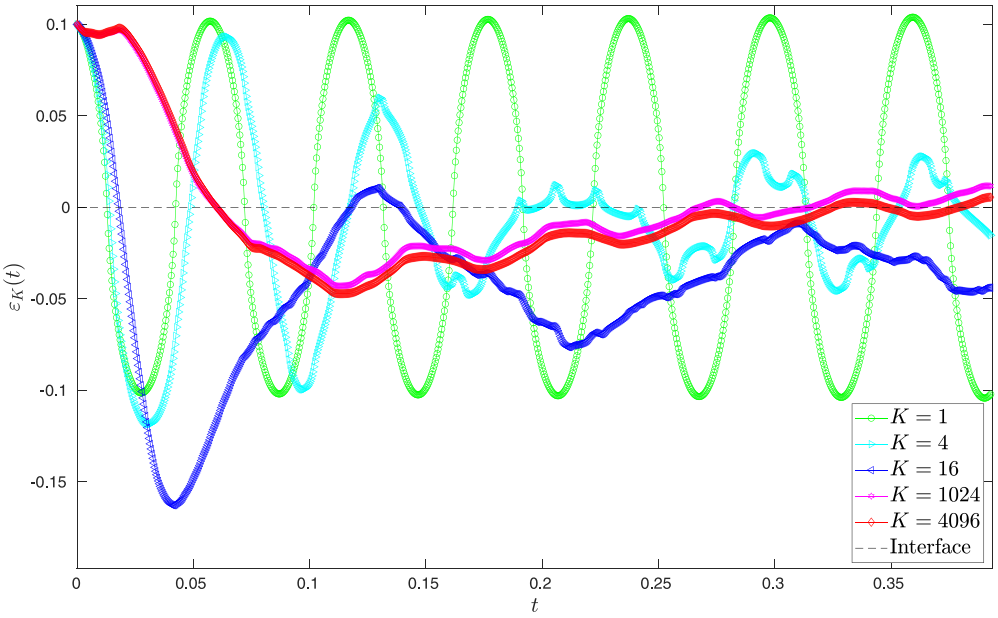

Figure 9. Experiment 2. Graph of $t \mapsto \epsilon_K(t)$, to $t \in [0, \pi/16]$ and $K = 1, 4, 16, 1024, 4096$.

approximation scheme was then applied to model and simulate the dynamics of edge states in photonic graphene. In this case, the presence of a domain interface was modelled by a space-dependent mass term. According to our theoretical framework, such terms also give rise to an effective force that controls electron trajectories. We demonstrated analytically and numerically that the latter oscillates about the interface, thus forming quasi-edge states.

In the future, the technique developed in this article will be used to design structures aiming at the control of electrons in Dirac matter. Indeed, evaluating the classical trajectories is more efficient and sometimes, leads to more insights into the electron behavior than a full numerical solution of the Dirac equation in curved space, as long as the conditions for the semi-classical approximation are fulfilled. Also, as the electromagnetic field is included in our theoretical description, our approach could be used to study the electromagnetic response of strained materials. Therefore, our work may have implications for important applications in nanoelectronics and photonics.

Data availability statement

No new data were created or analysed in this study.

Acknowledgments

The authors would like to thank Dr Pierre Lévesque for numerous discussions on Dirac materials and Prof. Lihui Chai for enlighting discussions on semi-classical analysis. This research was enabled in part by support provided by the Digital Research Alliance of Canada (alliancecan.ca).

Appendix. Properties of the projection operator

In this appendix, we present some intermediate technical results allowing for the derivation of the semi-classical limit of the Dirac equation. It is convenient to define the following operators.

$$\mathcal{D}(\boldsymbol{x},\boldsymbol{\pi}) := \bar{\alpha}^i(\boldsymbol{x})\pi_i + \beta\tilde{m}_D(\boldsymbol{x}) + \tilde{V}(\boldsymbol{x}), \tag{A1}$$

$$\mathcal{D}_0(\boldsymbol{x},\boldsymbol{\pi}) := \bar{\alpha}^i(\boldsymbol{x})\pi_i + \beta\tilde{m}_D(\boldsymbol{x}), \tag{A2}$$

$$\Pi_\pm(\boldsymbol{x},\boldsymbol{\pi}) := \frac{1}{2}\left[1 \pm \frac{\mathcal{D}_0(\boldsymbol{x},\boldsymbol{\pi})}{\lambda(\boldsymbol{x},\boldsymbol{\pi})}\right], \tag{A3}$$

where

$$h_\pm(\boldsymbol{x},\boldsymbol{\pi}) := \pm\lambda(\boldsymbol{x},\boldsymbol{\pi}) + \tilde{V}(\boldsymbol{x}), \tag{A4}$$

$$\lambda(\boldsymbol{x},\boldsymbol{\pi}) := \sqrt{g^{ij}\pi_i\pi_j + \tilde{m}_D^2(\boldsymbol{x})}, \tag{A5}$$

$$\boldsymbol{\omega}_\pm(\boldsymbol{x},\boldsymbol{\pi}) := \pm\frac{\boldsymbol{\pi}}{\lambda(\boldsymbol{x},\boldsymbol{\pi})} = \nabla_{\boldsymbol{p}} h_\pm(\boldsymbol{x},\boldsymbol{\pi}), \tag{A6}$$

and the Dirac matrices in the mostly-minus metric is related to those in the mostly-plus metric as $\bar{\alpha}^i := \bar{\alpha}^i_{+---} = -\bar{\alpha}^i_{-+++}$. The following properties will be proven hereafter

$$\Pi_\pm^2 = \Pi_\pm, \tag{A7}$$

$$\Pi_\pm\Pi_\mp = 0, \tag{A8}$$

$$\mathcal{D} = h_+\Pi_+ + h_-\Pi_-, \tag{A9}$$

$$\Pi_\pm\mathcal{D} = h_\pm\Pi_\pm, \tag{A10}$$

$$\Pi_\pm\bar{\alpha}^i(\boldsymbol{x})\Pi_\pm = \omega_\pm^i\Pi_\pm, \tag{A11}$$

$$\bar{\alpha}^i(\boldsymbol{x})\Pi_\pm = \Pi_\mp\bar{\alpha}^i(\boldsymbol{x}) + \omega_\pm^i. \tag{A12}$$

We first have.

Property 1. $\mathcal{D}_0^2 = \lambda^2\mathbb{I}$.

Proof. We have

$$\begin{aligned}\mathcal{D}_0^2 &= \left[\bar{\alpha}^i\pi_i + \tilde{m}_D\beta\right]\left[\bar{\alpha}^j\pi_j + \tilde{m}_D\beta\right],\\ &= \bar{\alpha}^i\bar{\alpha}^j\pi_i\pi_j + \tilde{m}_D^2\mathbb{I} + \bar{\alpha}^i\pi_i\tilde{m}_D\beta + \tilde{m}_D\beta\bar{\alpha}^j\pi_j,\\ &= \alpha^a\alpha^b e^i_a e^j_b\pi_i\pi_j + \tilde{m}_D^2\mathbb{I} + m\pi_i e^i_a\left(\beta\alpha^a + \alpha^a\beta\right).\\ &= \alpha^a\alpha^b\bar{\pi}_a\bar{\pi}_b + \tilde{m}_D^2\mathbb{I}.\end{aligned}$$

The last term is zero using anticommutation of Dirac matrices. For the first term, we use

$$\alpha^a\alpha^b = \delta^{ab}\mathbb{I} + 2\mathtt{i}\epsilon^{abc}\mathcal{S}^c. \tag{A13}$$

We get

$$\begin{aligned}\mathcal{D}_0^2 &= \left(\bar{\pi}_a\bar{\pi}^a + \tilde{m}_D^2\right)\mathbb{I},\\ &= \left(g^{ij}\pi_i\pi_j + \tilde{m}_D^2\right)\mathbb{I} = \lambda^2\mathbb{I}.\end{aligned}$$

This concludes the proof. □

Then, we can show that $\Pi_\pm$ are projection operators:

Property 2. $\Pi_\pm^2 = \Pi_\pm$ and $\Pi_\pm\Pi_\mp = 0$.

Proof. We have

$$\begin{aligned}\Pi_\pm^2 &= \frac{1}{4}\left[1 \pm \frac{\mathcal{D}_0}{\lambda}\right]\left[1 \pm \frac{\mathcal{D}_0}{\lambda}\right],\\ &= \frac{1}{4}\left[1 + \frac{\mathcal{D}_0^2}{\lambda^2} \pm 2\frac{\mathcal{D}_0}{\lambda}\right],\\ &= \frac{1}{2}\left[1 \pm \frac{\mathcal{D}_0}{\lambda}\right] = \Pi_\pm.\end{aligned}$$

Moreover we have:

$$\begin{aligned}\Pi_\pm\Pi_\mp &= \frac{1}{4}\left[1 \pm \frac{\mathcal{D}_0}{\lambda}\right]\left[1 \mp \frac{\mathcal{D}_0}{\lambda}\right],\\ &= \frac{1}{4}\left[1 - \frac{\mathcal{D}_0^2}{\lambda^2} \pm \frac{\mathcal{D}_0}{\lambda} \mp \frac{\mathcal{D}_0}{\lambda}\right] = 0.\end{aligned}$$

This concludes the proof. □

We now demonstrate two other important properties:

Property 3. $\Pi_\pm\mathcal{D} = h_\pm\Pi_\pm$.

Proof. We start from

$$\begin{aligned}\Pi_\pm\mathcal{D} &= \Pi_\pm\mathcal{D}_0 + \Pi_\pm\tilde{V},\\ &= \frac{1}{2}\left[1 \pm \frac{\mathcal{D}_0}{\lambda}\right]\mathcal{D}_0 + \Pi_\pm\tilde{V},\\ &= \frac{1}{2}\left[\mathcal{D}_0 \pm \lambda\right] + \Pi_\pm\tilde{V},\\ &= \pm\lambda\frac{1}{2}\left[1 \pm \frac{\mathcal{D}_0}{\lambda}\right] + \Pi_\pm\tilde{V} = h_\pm\Pi_\pm.\end{aligned}$$

Incidently, we also have that $\Pi_\pm\mathcal{D}_0 = \pm\lambda\Pi_\pm$. This concludes the proof. □

Property 4. $\Pi_\pm\bar{\alpha}^i\Pi_\pm = \omega_\pm^i\Pi_\pm$.

Proof. We start from

$$\begin{aligned}\Pi_\pm\bar{\alpha}^i\Pi_\pm &= \frac{1}{4}\left[1 \pm \frac{\mathcal{D}_0}{\lambda}\right]\bar{\alpha}^i\left[1 \pm \frac{\mathcal{D}_0}{\lambda}\right],\\ &= \frac{1}{4}\left[\bar{\alpha}^i \pm \bar{\alpha}^i\frac{\mathcal{D}_0}{\lambda} \pm \frac{\mathcal{D}_0}{\lambda}\bar{\alpha}^i + \frac{\mathcal{D}_0\bar{\alpha}^i\mathcal{D}_0}{\lambda^2}\right].\end{aligned}$$

We have that

$$\bar{\alpha}^i\mathcal{D}_0 = \alpha^b e^i_b \left[\alpha^a \bar{\pi}_a + \tilde{m}_D\beta\right], \tag{A14}$$
$$= e^i_b \left[\alpha^b\alpha^a\bar{\pi}_a - \tilde{m}_D\beta\alpha^b\right], \tag{A15}$$
$$= 2e^i_b\bar{\pi}_a\delta^{ab}\mathbb{I} - \mathcal{D}_0\bar{\alpha}^i = 2\pi^i - \mathcal{D}_0\bar{\alpha}^i. \tag{A16}$$

Then, we have

$$\bar{\alpha}^i\mathcal{D}_0 + \mathcal{D}_0\bar{\alpha}^i = 2\pi^i,$$
$$\mathcal{D}_0\bar{\alpha}^i\mathcal{D}_0 = 2\mathcal{D}_0\pi^i - \lambda^2\bar{\alpha}^i.$$

Hence

$$\Pi_\pm\bar{\alpha}^i\Pi_\pm = \frac{\pi^i}{2\lambda}\left[\pm 1 + \frac{\mathcal{D}_0}{\lambda}\right],$$
$$= \pm\frac{\pi^i}{2\lambda}\left[1 \pm \frac{\mathcal{D}_0}{\lambda}\right] = \omega^i_\pm\Pi_\pm.$$

This concludes the proof. □

Property 5. $\bar{\alpha}^i\Pi_\pm = \Pi_\mp + \omega^i_\pm$.

Proof. Using (A14), we get

$$\bar{\alpha}^i\Pi_\pm = \bar{\alpha}^i\frac{1}{2}\left[1 \pm \frac{\mathcal{D}_0}{\lambda}\right],$$
$$= \frac{1}{2}\left[\bar{\alpha}^i \pm \frac{2\pi^i - \mathcal{D}_0\bar{\alpha}^i}{\lambda}\right],$$
$$= \frac{1}{2}\left[1 \mp \frac{\mathcal{D}_0\bar{\alpha}^i}{\lambda}\right]\bar{\alpha}^i \pm \frac{\pi^i}{\lambda} = \Pi_\mp\bar{\alpha}^i + \omega^i_\pm.$$

This concludes the proof. □

ORCID iDs

François Fillion-Gourdeau https://orcid.org/0009-0003-5433-7477
Emmanuel Lorin https://orcid.org/0000-0001-8854-4739
Xu Yang https://orcid.org/0000-0001-6239-1922

References

[1] Wehling T O, Black-Schaffer A M and Balatsky A V 2014 Dirac materials *Adv. Phys.* **63** 1–76
[2] Cayssol J 2013 Introduction to Dirac materials and topological insulators *C. R. Phys.* **14** 760–78
[3] Wallace P R 1947 The band theory of graphite *Phys. Rev.* **71** 622–34
[4] Geim A K and Novoselov K S 2009 The rise of graphene *Nanoscience and Technology* (World Scientific) pp 11–19
[5] Castro Neto A H, Guinea F, Peres N M R, Novoselov K S and Geim A K 2009 The electronic properties of graphene *Rev. Mod. Phys.* **81** 109–62
[6] Hasan M Z and Kane C L 2010 *Colloquium*: Topological insulators *Rev. Mod. Phys.* **82** 3045–67
[7] Bansil A, Lin H and Das T 2016 *Colloquium*: Topological band theory *Rev. Mod. Phys.* **88** 021004

[8] Qi X-L and Zhang S-C 2011 Topological insulators and superconductors *Rev. Mod. Phys.* **83** 1057–110
[9] Armitage N P, Mele E J and Vishwanath A 2018 Weyl and Dirac semimetals in three-dimensional solids *Rev. Mod. Phys.* **90** 015001
[10] Balatsky A V, Vekhter I and Zhu J-X 2006 Impurity-induced states in conventional and unconventional superconductors *Rev. Mod. Phys.* **78** 373–433
[11] Volovik G E 1992 *Exotic Properties of Superfluid Helium 3* vol 1 (World Scientific)
[12] Uehlinger T, Jotzu G, Messer M, Greif D, Hofstetter W, Bissbort U and Esslinger T 2013 Artificial graphene with tunable interactions *Phys. Rev. Lett.* **111** 185307
[13] Raghu S and Haldane F D M 2008 Analogs of quantum-Hall-effect edge states in photonic crystals *Phys. Rev.* A **78** 033834
[14] Sepkhanov R A, Bazaliy Y B and Beenakker C W J 2007 Extremal transmission at the Dirac point of a photonic band structure *Phys. Rev.* A **75** 063813
[15] Zhang X 2008 Observing zitterbewegung for photons near the Dirac point of a two-dimensional photonic crystal *Phys. Rev. Lett.* **100** 113903
[16] Rechtsman M C, Plotnik Y, Zeuner J M, Song D, Chen Z, Szameit A and Segev M 2013 Topological creation and destruction of edge states in photonic graphene *Phys. Rev. Lett.* **111** 103901
[17] Khanikaev A B, Mousavi S H, Tse W-K, Kargarian M, MacDonald A H and Shvets G 2013 Photonic topological insulators *Nat. Mater.* **12** 233–9
[18] Mousavi S H, Khanikaev A B and Wang Z 2015 Topologically protected elastic waves in phononic metamaterials *Nat. Commun.* **6** 1–7
[19] Braun J W, Su Q and Grobe R 1999 Numerical approach to solve the time-dependent Dirac equation *Phys. Rev.* A **59** 604–12
[20] Succi S and Benzi R 1993 Lattice Boltzmann equation for quantum mechanics *Physica* D **69** 327–32
[21] Fillion-Gourdeau F, Lorin E and Bandrauk A D 2012 Numerical solution of the time-dependent Dirac equation in coordinate space without fermion-doubling *Comput. Phys. Commun.* **183** 1403–15
[22] Bao W and Li X-G 2004 An efficient and stable numerical method for the Maxwell–Dirac system *J. Comput. Phys.* **199** 663–87
[23] Hammer R, Pötz W and Arnold A 2014 A dispersion and norm preserving finite difference scheme with transparent boundary conditions for the Dirac equation in $(1+1)$d *J. Comput. Phys.* **256** 728–47
[24] Hammer R and Pötz W 2014 Staggered grid leap-frog scheme for the $(2+1)$d Dirac equation *Comput. Phys. Commun.* **185** 40–52
[25] Pötz W 2017 Single-cone finite-difference schemes for the $(2+1)$-dimensional Dirac equation in general electromagnetic textures *Phys. Rev.* E **96** 053312
[26] Antoine X, Fillion-Gourdeau F, Lorin E and MacLean S 2020 Pseudospectral computational methods for the time-dependent Dirac equation in static curved spaces *J. Comput. Phys.* **411** 109412
[27] Fillion-Gourdeau F, Lorin E and MacLean S 2021 Numerical quasiconformal transformations for electron dynamics on strained graphene surfaces *Phys. Rev.* E **103** 013312
[28] Flouris K, Mendoza Jimenez M, Debus J-D and Herrmann H J 2018 Confining massless Dirac particles in two-dimensional curved space *Phys. Rev.* B **98** 155419
[29] Maslov V P and Fedoriuk M V 1981 *Semi-Classical Approximation in Quantum Mechanics* vol 7 (D. Reidel Publishing Company)
[30] Bolte J and Keppeler S 1999 A semiclassical approach to the Dirac equation *Ann. Phys., NY* **274** 125–62
[31] Spohn H 2000 Semiclassical limit of the Dirac equation and spin precession *Ann. Phys., NY* **282** 420–31
[32] Sparber C and Markowich P 2003 Semiclassical asymptotics for the Maxwell-Dirac system *J. Math. Phys.* **44** 4555–72
[33] Reijnders K J A, Tudorovskiy T and Katsnelson M I 2013 Semiclassical theory of potential scattering for massless Dirac fermions *Ann. Phys., NY* **333** 155–97
[34] Bolte J and Keppeler S 1998 Semiclassical time evolution and trace formula for relativistic spin-1/2 particles *Phys. Rev. Lett.* **81** 1987–91
[35] Bøggild P, Caridad J M, Stampfer C, Calogero G, Papior N R and Brandbyge M 2017 A two-dimensional Dirac fermion microscope *Nat. Commun.* **8** 1–12
[36] Carmier P and Ullmo D 2008 Berry phase in graphene: semiclassical perspective *Phys. Rev.* B **77** 245413

[37] Reijnders K J A, Minenkov D S, Katsnelson M I and Dobrokhotov S 2018 Electronic optics in graphene in the semiclassical approximation *Ann. Phys., NY* **397** 65–135
[38] Paredes-Rocha E, Betancur-Ocampo Y, Szpak N and Stegmann T 2021 Gradient-index electron optics in graphene $p-n$ junctions *Phys. Rev.* B **103** 045404
[39] Reijnders K J A and Katsnelson M I 2017 Diffraction catastrophes and semiclassical quantum mechanics for Veselago lensing in graphene *Phys. Rev.* B **96** 045305
[40] Silenko A J and Teryaev O V 2005 Semiclassical limit for Dirac particles interacting with a gravitational field *Phys. Rev.* D **71** 064016
[41] Gosselin P, Bérard A and Mohrbach H 2007 Semiclassical dynamics of Dirac particles interacting with a static gravitational field *Phys. Lett.* A **368** 356–61
[42] Cianfrani F and Montani G 2008 Curvature-spin coupling from the semi-classical limit of the Dirac equation *Int. J. Mod. Phys.* A **23** 1274–7
[43] Cianfrani F and Montani G 2008 Dirac equations in curved space-time vs. Papapetrou spinning particles *Europhys. Lett.* **84** 30008
[44] Oancea M A and Kumar A 2023 Semiclassical analysis of Dirac fields on curved spacetime *Phys. Rev.* D **107** 044029
[45] de Juan F, Mañes J L and Vozmediano M A H 2013 Gauge fields from strain in graphene *Phys. Rev.* B **87** 165131
[46] Vozmediano M A H, Katsnelson M I and Guinea F 2010 Gauge fields in graphene *Phys. Rep.* **496** 109–48
[47] de Juan F, Sturla M and Vozmediano M A H 2012 Space dependent Fermi velocity in strained graphene *Phys. Rev. Lett.* **108** 227205
[48] Volovik G E and Zubkov M A 2014 Emergent Horava gravity in graphene *Ann. Phys., NY* **340** 352–68
[49] Amorim B *et al* 2016 Novel effects of strains in graphene and other two dimensional materials *Phys. Rep.* **617** 1–54
[50] Oliva-Leyva M and Naumis G G 2015 Generalizing the Fermi velocity of strained graphene from uniform to nonuniform strain *Phys. Lett.* A **379** 2645–51
[51] Naumis G G, Barraza-Lopez S, Oliva-Leyva M and Terrones H 2017 Electronic and optical properties of strained graphene and other strained 2D materials: a review *Rep. Prog. Phys.* **80** 096501
[52] Stegmann T and Szpak N 2016 Current flow paths in deformed graphene: from quantum transport to classical trajectories in curved space *New J. Phys.* **18** 053016
[53] Lee-Thorp J P, Weinstein M I and Zhu Y 2019 Elliptic operators with honeycomb symmetry: Dirac points, edge states and applications to photonic graphene *Arch. Ration. Mech. Anal.* **232** 1–63
[54] Pollock M D 2010 On the Dirac equation in curved space-time *Acta Phys. Pol.* B **41** 1827–46
[55] Arias E, Hernández A R and Lewenkopf C 2015 Gauge fields in graphene with nonuniform elastic deformations: a quantum field theory approach *Phys. Rev.* B **92** 245110
[56] Huang Z, Jin S, Wu H and Yin D 2012 Gaussian beam methods for the Dirac equation in the semiclassical regime *Commun. Math. Sci.* **10** 1301–15
[57] Houchmandzadeh B 2020 The Hamilton–Jacobi equation: an alternative approach *Am. J. Phys.* **88** 353–9
[58] Gallerati A 2019 Graphene properties from curved space Dirac equation *Eur. Phys. J. Plus* **134** 202
[59] Guinea F, Geim A K, Katsnelson M I and Novoselov K S 2010 Generating quantizing pseudomagnetic fields by bending graphene ribbons *Phys. Rev.* B **81** 035408
[60] Pereira V M and Castro N A H 2009 Strain engineering of graphene's electronic structure *Phys. Rev. Lett.* **103** 046801
[61] Chaves A J, Frederico T, Oliveira O, de Paula W and Santos M C 2014 Optical conductivity of curved graphene *J. Phys.: Condens. Matter* **26** 185301
[62] Groth C W, Wimmer M, Akhmerov A R and Waintal X 2014 Kwant: a software package for quantum transport *New J. Phys.* **16** 063065
[63] Jakob W, Rhinelander J, and Moldovan D 2016 pybind11—seamless operability between C++11 and Python (available at: https://github.com/pybind/pybind11)
[64] Lorin E and Yang X 2024 Quasi-optimal domain decomposition method for neural network-based computation of the time-dependent Schrödinger equation *Comput. Phys. Commun.* **299** 109129
[65] Hu P, Hong L and Zhu Y 2020 Linear and nonlinear electromagnetic waves in modulated honeycomb media *Stud. Appl. Math.* **144** 18–45
[66] Hairer E, Lubich C and Wanner G 2003 Geometric numerical integration illustrated by the Störmer-Verlet method *Acta Numer.* **12** 399–450